Table 1
Antiviral activity of C-HR-derived peptides against gp41 recombinant viruses.

	EC_{50} (nM)					
	T-20	T-20_{S138A}	T-20EK	C34	$C34_{N126K}$	SC35EK
HIV-1_{WT} [a]	2.4 ± 0.6	0.6 ± 0.1	1.9 ± 0.5	2.1 ± 0.7	1.6 ± 0.5	2.4 ± 0.9
HIV-1_{I37N}	47 ± 6.9 (**20**)	4.3 ± 1.3 (7.2)	21 ± 2.4 (**11**)	3.3 ± 1.1(1.6)	1.9 ± 0.1 (1.2)	1.0 ± 0.4(0.4)
HIV-1_{L44M}	4.1 ± 1.2 (1.7)	0.7 ± 0.2 (1.2)	2.2 ± 0.6 (1.2)	1.1 ± 0.3(0.5)	0.8 ± 0.2 (0.5)	0.6 ± 0.2(0.3)
HIV-1_{N126K}	4.4 ± 1.3 (1.8)	1.2 ± 0.4 (2.0)	2.8 ± 0.2 (1.5)	6.3 ± 1.2(3.0)	1.5 ± 0.2 (0.9)	3.3 ± 0.2(1.4)
HIV-$1_{I37N/N126K}$	660 ± 180(**275**)	16 ± 4.8 (**27**)	14 ± 5.1 (7.4)	20 ± 4.5(9.5)	3.4 ± 0.4 (2.1)	2.9 ± 0.3(1.2)
HIV-$1_{I37N/L44M/N126K}$	>1000 (>417)	130 ± 40(220)	240 ± 95(126)	66 ± 23 (31)	4.0 ± 0.8 (2.5)	1.1 ± 0.1(0.5)
HIV-1_{L33S}	23 ± 5.5 (9.6)	3.1 ± 0.6 (5.2)	13 ± 2.6 (6.8)	3.2 ± 1.1(1.5)	2.1 ± 0.1 (1.3)	3.0 ± 0.8(1.2)
HIV-1_{N43D}	49 ± 10 (**20**)	3.5 ± 0.9 (5.8)	4.1 ± 1.2 (2.2)	4.4 ± 0.4(2.1)	1.4 ± 0.1 (0.8)	0.4 ± 0.2(0.2)
HIV-1_{I69L}	2.1 ± 0.5 (0.9)	0.5 ± 0.2 (0.8)	2.2 ± 0.4 (1.2)	2.7 ± 0.2(1.3)	2.2 ± 0.5 (1.4)	2.7 ± 0.5(1.1)
HIV-1_{E137K}	2.0 ± 0.3 (0.8)	0.7 ± 0.1 (1.2)	2.5 ± 0.4 (1.3)	2.6 ± 0.2(1.2)	2.3 ± 0.7 (1.4)	3.1 ± 0.8(1.3)
HIV-$1_{N43D/S138A}$	84 ± 16 (**35**)	3.2 ± 1.0 (5.3)	3.4 ± 1.1 (1.8)	2.7 ± 0.2(1.3)	1.6 ± 0.5 (1.0)	0.3 ± 0.1(0.1)
HIV-$1_{L33S/N43D/S138A}$	>1000 (**>417**)	550 ± 72(**174**)	330 ± 94 (14)	30 ± 9.2(2.6)	4.2 ± 1.2 (0.4)	0.9 ± 0.3(0.4)
HIV-$1_{N43D/E137K/S138A}$	110 ± 31 (**46**)	14 ± 4.7 (**23**)	7.0 ± 2.4 (3.7)	7.4 ± 1.9(3.5)	2.1 ± 0.7 (1.3)	1.9 ± 0.6(0.8)
HIV-$1_{L33S/N43D/E137K/S138A}$	>1000 (**>417**)	>1000(**>1667**)	>1000 (**>526**)	31 ± 5.0 (**15**)	6.7 ± 1.7 (4.2)	1.2 ± 0.2(0.5)
HIV-$1_{L33S/N43D/I69L/E137K/S138A}$	>1000 (**>417**)	>1000(**>1667**)	>1000 (**>526**)	50 ± 12 (**24**)	28 ± 7.1(**17.5**)	1.0 ± 0.9(0.4)

Anti-HIV activity was determined using the MAGI assay. Fifty percent effective concentration (EC_{50}) values and SD were obtained from the results of at least three independent experiments. Shown in parentheses are the fold-increases in resistance (increase in EC_{50} value) calculated by comparison to a wild-type virus (HIV-1_{WT}). Increases of over 10-fold are indicated in bold.

[a] To improve the replication kinetics, substitution of D36G, observed in majority of HIV-1 strains, was introduced into the NL4-3 background used in this study (wild-type virus; HIV-1_{WT}) (Izumi et al., 2009; Mink et al., 2005).

observed in wild-type HIV-1 as polymorphisms (Kuiken et al., 2010; Loutfy et al., 2007), conferred little resistance to all peptide fusion inhibitors tested. However, introduction of L44M to HIV-$1_{I37N/N126K}$ (HIV-$1_{I37N/L44M/N126K}$) remarkably enhanced resistance to T-20 derivatives. This was consistent with previous studies that also reported a resistance enhancement (1.8-fold) by L44M to T-20 (Loutfy et al., 2007). Collectively, these data suggest that L44M has as a role in HIV-1 resistance as a secondary mutation. All peptides sufficiently suppressed HIV-1_{I69L}, suggesting that I69L may be a secondary mutation or a polymorphism. N126K conferred only marginal resistance (<3-fold) to all peptide fusion inhibitors, but in the background of I37N (HIV-$1_{I37N/N126K}$) it enhanced resistance to T-20, T-20_{S138A}, and C34. L33S, which was originally reported as a C34 resistance associated mutation (Armand-Ugon et al., 2003), significantly enhanced resistance in the background of N43D/S138A mutations (HIV-$1_{L33S/N43D/S138A}$). Similar to the N126K mutation, E137K also enhanced resistance by N43D/S138A (HIV-$1_{N43D/E137K/S138A}$) and L33S/N43D/S138A (HIV-$1_{L33S/N43D/E137K/S138A}$) to T-$20_{S138A}$, T-20, and T-20EK. These results indicate that L33S and I37N appear to be primary mutations for T-20 derivatives.

3.3. *Effect of substitutions in the gp120 on peptide susceptibility*

Polymorphisms in the gp120 that influence co-receptor usage may influence T-20 susceptibility (Labrosse et al., 2003; Reeves et al., 2002). Meanwhile, others reported that T-20 susceptibility was not influenced by co-receptor usage (Cilliers et al., 2004; Melby et al., 2006). Resistance induction experiments performed in this study revealed that most laboratory strains with *in vitro* resistance to fusion inhibitors acquired substitutions in both the gp120 and the gp41 (Armand-Ugon et al., 2003; Eggink et al., 2011; Fikkert et al., 2002; Izumi et al., 2010; Nameki et al., 2005; Shimura et al., 2010). However, most substitutions showed little impact on resistance, and only contributed to a small enhancement of replication capacity (Eggink et al., 2011; Izumi et al., 2010; Nameki et al., 2005; Shimura et al., 2010). In the present study, we examined peptide susceptibility of cloned viruses that contain all Env substitutions observed in the selection (both gp120 and gp41). Most substitutions in the gp120 attenuated resistance to fusion inhibitors (Table 3). Therefore, *in vitro* experiments showed that substitutions in the gp120 are not likely associated with resistance.

3.4. *Influence of mutations in the gp41 on HIV-1 replication*

To address the effects of mutations on HIV-1 replication, we examined the replication kinetics of T-20_{S138A}-resistant HIV-$1_{N43D/S138A}$ variants. Consistent with a previous report (Lohrengel et al., 2005), the L33S mutation did not significantly affect the replication kinetics and infectivity compared with those of HIV-1_{WT} (Fig. 2A). The S138A mutation restored the replication

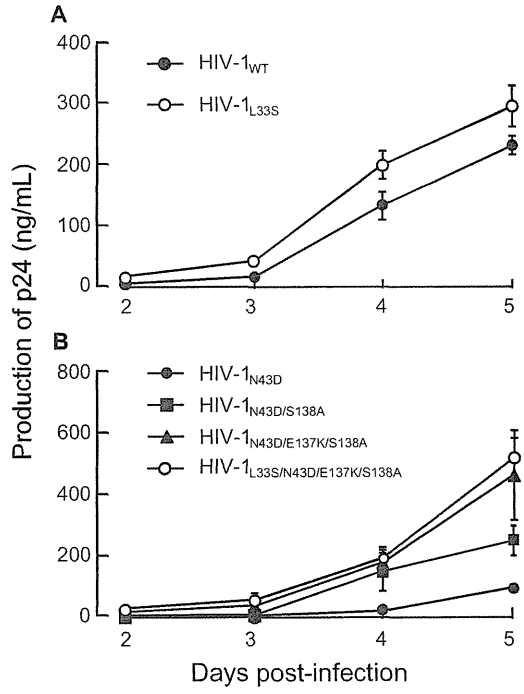

Fig. 2. Replication kinetics of T-20_{S138A}-resistant variants. Replication kinetics of T-20_{S138A}-resistant recombinant variants that introduced L33S mutation (A), or combinations of L33S, E137K, and S138A mutations in HIV-1_{N43D} (B). To improve replication kinetics, the D36G polymorphism was introduced into the NL4-3 background used in this study (HIV-1_{WT}). Supernatants from infected MT-2 cells were collected on days 2–7 and the amount of p24 produced was determined. Representative results are shown as mean values with standard deviations estimated from three independent experiments.

kinetics of HIV-1_{N43D} (Fig. 2B), as previously described (Izumi et al., 2009). E137K was also associated with N43D mutation *in vivo* (Svicher et al., 2008), and restored infectivity impaired by N43D (Tolstrup et al., 2007). Introduction of E137K into N43D/S138A enhanced the replication kinetics, and further addition of L33S to N43D/E137K/S138A resulted in equivalent replication kinetics compared with HIV-$1_{N43D/E137K/S138A}$ (Fig. 2B) as observed in HIV-1_{WT} based mutants. During the passage of HIV-$1_{N43D/S138A}$, a synonymous mutation at amino acid position L44, TTG to CTG, was observed. Interestingly, $L_{TTG}44L_{CTG}$ enhanced viral replication kinetics through enhanced stability of the Rev-responsive element (RRE) secondary structure (Ueno et al., 2009). Therefore, we examined the viral replication kinetics of mutants with $L_{TTG}44L_{CTG}$, and compared HIV-1_{WT}, with HIV-$1_{L44L\text{-}CTG}$, and HIV-$1_{L33S/N43D/L44L\text{-}CTG/E137K/S138A}$ with HIV-$1_{L33S/N43D/L44L\text{-}CTG/I69L/E137K/S138A}$. As expected, the presence of $L_{TTG}44L_{CTG}$ enhanced replication in all viruses. Surprisingly, mutants with resistance mutations showed enhanced replication kinetics as determined by the p24 production assay of culture supernatants (Fig. 4A). Therefore, we further examined infectivity using the MAGI assay and determined that the infectivity of resistance variants containing $L_{TTG}44L_{CTG}$ was reduced compared with HIV-1_{WT} (Fig. 4B). These results indicate that the primary mutation, L33S, possesses less ability to attenuate HIV-1 replication, while I69L, S138A, and E137K enhance replication kinetics of T-20-resistant HIV-1 to a comparable level of HIV-1_{WT}.

3.5. Circular dichroism

To clarify the effect of E137K substitutions on peptide binding, we examined the binding affinities of E137K-containing C-HR peptides to N-HR using CD analysis. CD spectra reveal the presence of stable α-helical structures of six-helix bundles that are required for biological activity and are thought to mechanistically and thermodynamically correlate with HIV-1 fusion (Bianchi et al., 2005). Since *in vitro* T-20 does not interact with the N36 peptide (amino acid positions 35–70 of the N-HR), we used instead peptide C34 with E137K and/or S138A substitutions (Fig. 1A). We found that mixtures of $C34_{E137K}$, $C34_{S138A}$, or $C34_{E137K/S138A}$ with N36 or $N36_{N43D}$ showed sufficient and comparable α-helicity at 25 °C (Fig. 3A and B). We also determined the thermal stability of the helical complexes formed by the N36 and C34 peptides, which is also an indication of the binding affinity of these peptides. Hence, we measured and compared the melting temperatures (T_m) of various complexes, which indicates the 50% disruption of the six-helix bundle (Fig. 3C). Complexes of N36 and C34 containing the S138A and E137K/S138A substitutions (N36/$C34_{S138A}$ and N36/$C34_{E137K/S138A}$, respectively), showed higher thermal stability than N36/C34. Similarly, S138A and E137K/S138A restored the binding affinity of C34 to $N36_{N43D}$. These results indicate that E137K acts as a compensatory mutation for the T-20_{S138A}-resistance primary mutation, causing enhancement of replication kinetics.

3.6. Antiviral activity of E137K-modified peptides

Recently, we demonstrated that introduction of the S138A secondary mutation to T-20 (T-20_{S138A}) enhanced binding to mutated N-HR and suppresses resistance of T-20-resistance variants (Izumi et al., 2009). Similarly, as shown in Fig. 3, E137K enhanced binding affinity with N-HR, suggesting that introduction of E137K to T-20 may enhance the antiviral activity of T-20. We synthesized T-20 and T-20_{S138A} variants containing the E137K change (T-20_{E137K} and T-$20_{E137K/S138A}$) (Fig. 1A) and examined their anti-HIV activity against T-20_{S138A}-resistant HIV-1 (Table 2). All peptides exhibited potent antiviral activity against HIV-1_{WT}. HIV-$1_{L33S/N43D/S138A}$ and HIV-$1_{I37N/L44M/N126K}$ showed high resistance to T-20_{E137K},

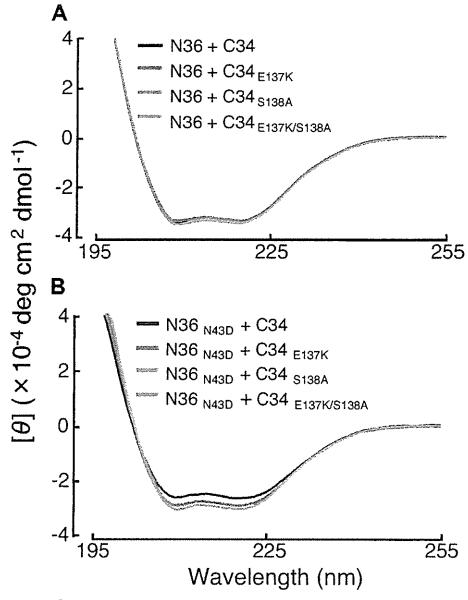

C

	T_m (°C)	
	N36	$N36_{N43D}$
C34	67.6	53.2
$C34_{E137K}$	68.9	56.7
$C34_{S138A}$	73.2	58.0
$C34_{E137K/S138A}$	74.6	63.3

Fig. 3. CD spectra (A and B) and thermal stability (C) of N36/C34 complexes. Peptide sequences used in this study are shown in FIG 1A and have also been previously described (Izumi et al., 2009). CD spectra of $C34_{E137K}$, $C34_{S138A}$, and $C34_{E137K/S138A}$ complexes with N36 (A) and $N36_{N43D}$ (B) are shown. Equimolar amounts (10 μM) of the N- and C-HR peptides were incubated at 37 °C for 30 min in PBS. The CD spectra of each mixture were then collected at 25 °C using a Jasco (Model J-710) spectropolarimeter. (C) Thermal stabilities, defined as the midpoint of the thermal unfolding transition (T_m) values, of the potential six-helix bundles of N- and C-HR peptides, were determined.

indicating that the resistance mechanism of T-20_{E137K} is similar to that of T-20_{S138A}. On the other hand, T-$20_{E137K/S138A}$ (Table 2) maintained some antiviral activity against HIV-$1_{L33S/N43D/S138A}$, HIV-$1_{L33S/N43D/E137K/S138A}$, and HIV-$1_{I37N/L44M/N126K}$ compared with other T-20 derivatives including electrostatically constrained T-20EK (Table 1 and Fig. 1). $C34_{E137K}$ and $C34_{E137K/S138A}$ significantly suppressed all HIV-1 variants tested except for HIV-$1_{I37N/L44M/N126K}$ by $C34_{E137K}$. These results indicate that peptides with resistant mutations may sustain their activity against particular resistant variants.

4. Discussion

The current study describes the introduction of resistance changes into the original and modified (T-20_{S138A}) versions of the T-20 peptide-fusion inhibitor. We analyzed the new T-20 derivatives using both wild-type and T-20-resistant strains. We also identified through dose escalation experiments, T-20_{S138A}-resistants. We found that T-20_{S138A}-resistant HIV-1 showed cross-resistance only to the T-20 derivatives, but not to C34 derivatives. Through the CD analysis, the N126K and E137K mutations in the C-HR may act as compensatory mutations for impaired interaction by a primary mutation, I37N and N43D in the N-HR, respectively. Since E137K is located within the T-20 sequence, we synthesized and characterized the activity of novel T-20-based peptides containing E137K (T-20_{E137K}). Here we demonstrate that

Table 2
Antiviral activity of E137K-induced C-HR peptides against T-20_{S138A}-resistant variants.

	EC_{50} (nM)			
	T-20_{E137K}	T-$20_{E137K/S138A}$	$C34_{E137K}$	$C34_{E137K/S138A}$
HIV-1_{WT} [a]	0.8 ± 0.2	0.5 ± 0.1	1.0 ± 0.3	0.7 ± 0.2
HIV-1_{L33S}	13 ± 3.2 (**16**)	2.2 ± 0.4 (4.5)	0.7 ± 0.2(0.7)	0.5 ± 0.1(0.7)
HIV-$1_{N43D/S138A}$	4.2 ± 0.7 (5.3)	0.7 ± 0.2 (1.4)	0.3 ± 0.1(0.3)	0.4 ± 0.1(0.6)
HIV-$1_{L33S/N43D/S138A}$	700 ± 150 (**880**)	45 ± 9.9 (**90**)	2.3 ± 0.4(2.3)	0.5 ± 0.2(0.7)
HIV-$1_{N43D/E137K/S138A}$	12 ± 3.6 (**15**)	2.4 ± 0.8 (4.8)	0.2 ± 0.1(0.2)	0.4 ± 0.1(0.6)
HIV-$1_{L33S/N43D/E137K/S138A}$	480 ± 47 (**600**)	36 ± 3.1 (**72**)	3.8 ± 1.3(3.8)	1.0 ± 0.4(1.4)
HIV-$1_{L33S/N43D/I69L/E137K/S138A}$	1808 ± 852(2260)	157 ± 83(314)	4 ± 2 (4)	1.0 ± 0.4(1.4)
HIV-$1_{I37N/L44M/N126K}$	200 ± 24 (**250**)	30 ± 8.7 (**60**)	17 ± 3.8 (**17**)	2.2 ± 0.3(3.1)

Anti-HIV activity was determined using the MAGI assay. Fifty percent effective concentration (EC_{50}) values and SD were obtained from the results of at least three independent experiments. Shown in parentheses are the fold-increases in resistance (increase in EC_{50} value) calculated by comparison to a wild-type virus (HIV-1_{WT}). Increases of over 10-fold are indicated in bold.

[a] To improve the replication kinetics, substitution of D36G, observed in majority of HIV-1 strains, was introduced into the NL4-3 background used in this study (wild-type virus; HIV-1_{WT}) (Izumi et al., 2009; Mink et al., 2005).

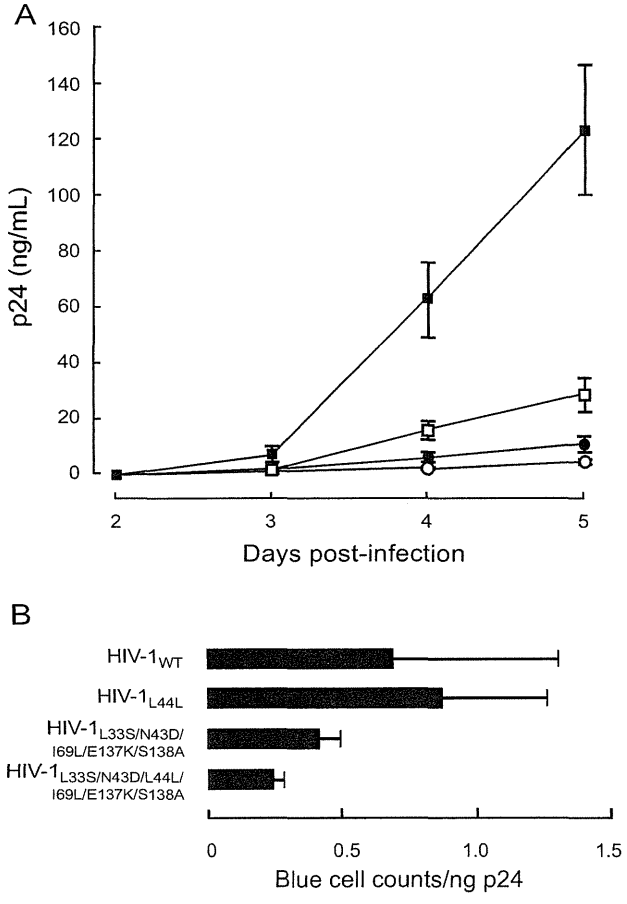

Fig. 4. Effect of secondary mutations in the N-HR on (A) replication kinetics and (B) infectivity. $L_{TTG}44L_{CTG}$ was introduced into HIV-1_{WT} and T-20_{S138A} resistant HIV-1 (HIV-$1_{L33S/N43D/L44L\text{-}CTG/I69L/E137K/S138A}$). Replication kinetics were determined by measuring p24 production in culture supernatants. HIV-1_{WT} (open circles), HIV-1_{L44L} (closed circles) HIV-$1_{L33S/N43D/I69L/E137K/S138A}$ (open squares), and HIV-$1_{L33S/N43D/L44L\text{-}CTG/I69L/E137K/S138A}$ (closed squares). $L_{TTG}44L_{CTG}$ introduction statistically enhanced both replication of HIV-1_{WT} and HIV-$1_{L33S/N43D/L44L\text{-}CTG/I69L/E137K/S138A}$ (Student's *t*-test, $p < 0.01$ on day 4 and 5). Relative infectivity (blue cell counts in MAGI cells divided by amount of p24) was calculated (B). Error bars indicate SD of three determinations. Decrease of infectivity between HIV-$1_{L33S/N43D/I69L/E137K/S138A}$ and HIV-$1_{L33S/N43D/L44L\text{-}CTG/I69L/E137K/S138A}$ were statistically significant (Student's *t*-test, $p < 0.05$).

the introduction of a secondary resistance mutation (E137K) in the backbone of a peptide fusion inhibitor is a useful change that results into more potent fusion inhibitors, even for HIV-1 strains that are resistant to peptide fusion inhibitors.

Selection of T-20_{S138A}-resistance starting with wild-type HIV-1 resulted in the emergence of I37N and L44M substitutions, which were located in the N-HR region that is thought to interact with T-20. Other substitutions at position 37 (I37T or I37K) also conferred resistance to T-20 and C34 (Nameki et al., 2005), suggesting that I37 in N-HR is critical for the attachment of C-HR-derived peptide fusion inhibitors. The L44M mutation has only been observed in subtype B HIV-1-infected patients treated with T-20 (Carmona et al., 2005), and conferred weak resistance to T-20 (Loutfy et al., 2007). In this study, L44M did not confer resistance to all peptide inhibitors; however, L44M in combination with other mutations (I37N/N126K) remarkably enhanced resistance to T-20_{S138A}, suggesting that L44M serves as a secondary mutation to enhance resistance to T-20_{S138A}. N126K also enhances resistance to some fusion inhibitors (Baldwin et al., 2004; Nameki et al., 2005; Eggink et al., 2008) by helping recover losses in intra-gp41 interactions that were caused by primary mutations, such as N43D.

When we selected T-20_{S138A}-resistant HIV-1 (HIV-$1_{N43D/S138A}$) we obtained a somehow different set of mutations that included L33S, which is located at the presumed T-20 binding site at N-HR, as well as I37N, N43D, and L44M. L33S was previously reported in HIV-1 variants resistant to T-20 (Fikkert et al., 2002), C34 (Armand-Ugon

Table 3
Antiviral activity of C-HR-derived peptides against gp160 recombinant viruses.

Compound	EC_{50} (nM)	
ddC	771 ± 272	
T-20 derivatives		
T20	>10,000	(NA)
T20EK	2729 ± 1113	(NA)
$T20_{S138A}$	3126 ± 453	(NA)
$T20_{E137K}$	2761 ± 1477	(NA)
$T20_{E137K/S138A}$	203 ± 54	(0.6)
C34 derivatives		
C34	171.0 ± 106	(3.4)
$C34_{N126K}$	25.9 ± 4.6	(NA)
SC34EK	1.0 ± 0.8	(1)
$C34_{E137K}$	7.0 ± 4.4	(0.4)
$C34_{E137K/S138A}$	0.3 ± 0.1	(0.3)

Anti-HIV activity was determined using the MAGI assay. Fifty percent effective concentration (EC_{50}) values and SD were obtained from the results of at least three independent experiments. Shown in parentheses are the fold-increases in resistance (increase in EC_{50} value) calculated by comparison to the resistant clone with mutations only in gp41 (HIV-$1_{L33S/N43D/I69L/E137K/S138A}$). To improve the replication kinetics, substitution of D36G, observed in majority of HIV-1 strains, was introduced into the NL4-3 background used in this study (Izumi et al., 2009; Mink et al., 2005). NA, not available; ddC, dideoxycytidine.

et al., 2003), and a membrane-anchored C-HR-derived peptide, M87 (Lohrengel et al., 2005). Although our work clearly demonstrates that L33S is involved in resistance to T-20 derivatives, it was not possible to discern whether L33S affected binding affinity to C-HR in the CD analyses because L33 was not in the sequence of the N36 N-HR peptide that we had to use in this study. As shown in Fig. 2, L33S did not significantly affect replication kinetics compared with HIV-1_{WT}, suggesting that L33S might sustain binding affinity with C-HR to form a stable six-helix bundle. The L33S mutation is located in the loop of stem IIc of the RRE (Ueno et al., 2009). Hence, nucleotide changes for L33S do not require compensatory mutations to maintain secondary structure of the RRE. Therefore, it is likely that L33S has little effect on replication kinetics. In this study, L33S conferred little resistance to C34 in this study, while it was previously reported to confer up to 10-fold resistance (Armand-Ugon et al., 2003), suggesting that some other viral background might affect the resistance, since Armand-Ugon et al. (2003) examined bulk virus samples obtained from the selection.

A prevalent polymorphism, E137K, which was associated with N43D *in vivo* (Svicher et al., 2008), has been proven to restore infectivity that has been impaired by N43D (Tolstrup et al., 2007). E137K did not affect susceptibility to all peptide fusion inhibitors by itself, but in combination with primary mutations, it remarkably enhanced resistance to T-20_{S138A}. Moreover, introduction of the E137K change into N43D/S138A enhanced the viral replication kinetics as shown in Fig. 2. A possible hydrogen bond between K137 and D43 may partially restore the reported loss in six-helix bundle stability conferred by the N43D mutation (Bai et al., 2008), suggesting that E137K can compensate for losses in the interactions between N-HR_{N43D} and C-HR. This hypothesis is consistent with our CD results presented in Fig. 3.

Because E137K restored binding affinity with N-HR similar to the S138A mutation, we expected that introduction of E137K into T-20 would effectively suppresses replication of T-20-resistant HIV-1. We examined the antiviral activity of E137K- and E137K/S138A-containing T-20 and C34 to T-20_{S138A}-resistant HIV-1. We found that T-20_{E137K} had similar antiviral activity with other T-20 derivatives such as T-20_{S138A} and T-$20_{E137K/S138A}$. Hence, we believe that the combination of few substitution secondary mutations can enhance the antiviral activity of peptide fusion inhibitors. Therefore, it is possible to design peptides that include the secondary mutations in the C-HR and use them by themselves and/or in combinations to block fusion inhibitor resistant viruses. Importantly, we have successfully applied this strategy to suppress HIV-1 resistance to next generation fusion inhibitor SC34EK (Shimura et al., 2010).

In this study, we identified two distinct pathways to escape pressure of T-20_{S138A}. Emergence of drug resistance mutants under drug pressure involves a stochastic selection. Nonetheless, the makeup of the final population depends on both the ability of specific populations to evade the drug, as well as their fitness that determines their representation in the escape population. There are several examples in the literature where HIV becomes resistant to the same drug by different mechanisms. For example, in the case of the most commonly used drugs that target HIV reverse transcriptase (RT), the virus can develop multidrug resistance by either the Q151M complex pathway (Kavlick et al., 1998; Shirasaka et al., 1995) or by accumulation of thymidine associated mutations (TAMs) (Hachiya et al., 2008; Kosalaraksa et al., 1999). We recently report some of background polymorphisms can also influence resistance pathways, such 172R/K in the RT region (Hachiya et al., 2012). In the case of the T-20S138A inhibitor, the N43D/S138A may also act as such polymorphisms despite the presence of primary mutations (Izumi et al., 2009) and preferentially affect the emergence of specific mutations.

5. Conclusion

As previously discussed (Izumi et al., 2009), although other developed peptide-based fusion inhibitors need many amino acid additions and/or substitutions for the enhancement of their antiviral activity (Chinnadurai et al., 2007; Eggink et al., 2008; Dwyer et al., 2007; Otaka et al., 2002), application of secondary mutations similar to T-20_{S138A} and T-$20_{E137K/S138A}$ is straightforward. It is based on information from viral evolution studies under drug pressure that help design improved inhibitors.

Acknowledgments

This work was supported by a grant from the Ministry of Education, Culture, Sports, Science, and Technology of Japan, a grant for the Promotion of AIDS Research from the Ministry of Health, Labour and Welfare. Additional support was by National Institute of Health (NIH) research Grants AI094715, AI076119, AI079801, and AI100890 (SGS). We are grateful to Biomedical Research Core (Tohoku University School of Medicine) for technical support. The authors declare non-financial competing interests.

References

Aquaro S, D'Arrigo R, Svicher V, Perri GD, Caputo SL, Visco-Comandini U, et al. Specific mutations in HIV-1 gp41 are associated with immunological success in HIV-1-infected patients receiving enfuvirtide treatment. Journal of Antimicrobial Chemotherapy 2006;58:714–22.

Armand-Ugon M, Gutierrez A, Clotet B, Este JA. HIV-1 resistance to the gp41-dependent fusion inhibitor C-34. Antiviral Research 2003;59:137–42.

Bai X, Wilson KL, Seedorff JE, Ahrens D, Green J, Davison DK, et al. Impact of the enfuvirtide resistance mutation N43D and the associated baseline polymorphism E137K on peptide sensitivity and six-helix bundle structure. Biochemistry 2008;47:6662–70.

Baldwin CE, Sanders RW, Deng Y, Jurriaans S, Lange JM, Lu M, et al. Emergence of a drug-dependent human immunodeficiency virus type 1 variant during therapy with the T20 fusion inhibitor. Journal of Virology 2004;78:12428–37.

Bianchi E, Finotto M, Ingallinella P, Hrin R, Carella AV, Hou XS, et al. Covalent stabilization of coiled coils of the HIV gp41N region yields extremely potent and broad inhibitors of viral infection. Proceedings of the National Academy of Sciences of the United States of America 2005;102:12903–8.

Cabrera C, Marfil S, Garcia E, Martinez-Picado J, Bonjoch A, Bofill M, et al. Genetic evolution of gp41 reveals a highly exclusive relationship between codons 36, 38 and 43 in gp41 under long-term enfuvirtide-containing salvage regimen. AIDS 2006;20:2075–80.

Cardoso RM, Brunel FM, Ferguson S, Zwick M, Burton DR, Dawson PE, et al. Structural basis of enhanced binding of extended and helically constrained peptide epitopes of the broadly neutralizing HIV-1 antibody 4E10. Journal of Molecular Biology 2007;365:1533–44.

Carmona R, Perez-Alvarez L, Munoz M, Casado G, Delgado E, Sierra M, et al. Natural resistance-associated mutations to enfuvirtide (T20) and polymorphisms in the gp41 region of different HIV-1 genetic forms from T20 naive patients. Journal of Clinical Virology 2005;32:248–53.

Chan DC, Chutkowski CT, Kim PS. Evidence that a prominent cavity in the coiled coil of HIV type 1 gp41 is an attractive drug target. Proceedings of the National Academy of Sciences of the United States of America 1998;95:15613–7.

Chan DC, Fass D, Berger JM, Kim PS. Core structure of gp41 from the HIV envelope glycoprotein. Cell 1997;89:263–73.

Chinnadurai R, Rajan D, Munch J, Kirchhoff F. Human immunodeficiency virus type 1 variants resistant to first- and second-version fusion inhibitors and cytopathic in ex vivo human lymphoid tissue. Journal of Virology 2007;81:6563–72.

Cilliers T, Patience T, Pillay C, Papathanasopoulos M, Morris L. Sensitivity of HIV type 1 subtype C isolates to the entry inhibitor T-20. AIDS Research and Human Retroviruses 2004;20:477–82.

Debnath AK, Radigan L, Jiang S. Structure-based identification of small molecule antiviral compounds targeted to the gp41 core structure of the human immunodeficiency virus type 1. Journal of Medicinal Chemistry 1999;42:3203–9.

Dwyer JJ, Wilson KL, Davison DK, Freel SA, Seedorff JE, Wring SA, et al. Design of helical, oligomeric HIV-1 fusion inhibitor peptides with potent activity against enfuvirtide-resistant virus. Proceedings of the National Academy of Sciences of the United States of America 2007;104:12772–7.

Dwyer JJ, Wilson KL, Martin K, Seedorff JE, Hasan A, Medinas RJ, et al. Design of an engineered N-terminal HIV-1 gp41 trimer with enhanced stability and potency. Protein Science 2008;17:633–43.

Eggink D, Baldwin CE, Deng Y, Langedijk JP, Lu M, Sanders RW, et al. Selection of T1249-resistant human immunodeficiency virus type 1 variants. Journal of Virology 2008;82:6678–88.

Eggink D, Bontjer I, Langedijk JP, Berkhout B, Sanders RW. Resistance of human immunodeficiency virus type 1 to a third-generation fusion inhibitor requires

multiple mutations in gp41 and is accompanied by a dramatic loss of gp41 function. Journal of Virology 2011;85:10785–97.
Eshleman SH, Hudelson SE, Bruce R, Lee T, Owens MR, Hackett J, et al. Analysis of HIV type 1 gp41 sequences in diverse HIV type 1 strains. AIDS Research and Human Retroviruses 2007;23:1593–8.
Fikkert V, Cherepanov P, Van Laethem K, Hantson A, Van Remoortel B, Pannecouque C, et al. env chimeric virus technology for evaluating human immunodeficiency virus susceptibility to entry inhibitors. Antimicrobial Agents and Chemotherapy 2002;46:3954–62.
Hachiya A, Kodama EN, Sarafianos SG, Schuckmann MM, Sakagami Y, Matsuoka M, Takiguchi M, Gatanaga H, Oka S. Amino acid mutation N348I in the connection subdomain of human immunodeficiency virus type 1 reverse transcriptase confers multiclass resistance to nucleoside and nonnucleoside reverse transcriptase inhibitors. Jouranl of Virology 2008;82:3261–70.
Hachiya A, Marchand B, Kirby KA, Michailidis E, Tu X, Palczewski K, Ong YT, Li Z, Griffin DT, Schuckmann MM, Tanuma J, Oka S, Singh K, Kodama EN, Sarafianos SG. HIV-1 reverse transcriptase (RT) polymorphism 172K suppresses the effect of clinically relevant drug resistance mutations to both nucleoside and non-nucleoside RT inhibitors. Journal of Biological Chemistry 2012;287:29988–99.
He Y, Xiao Y, Song H, Liang Q, Ju D, Chen X, et al. Design and evaluation of sifuvirtide, a novel HIV-1 fusion inhibitor. Journal of Biological Chemistry 2008;283:11126–34.
Izumi K, Kodama E, Shimura K, Sakagami Y, Watanabe K, Ito S, et al. Design of peptide-based inhibitors for human immunodeficiency virus type 1 strains resistant to T-20. Journal of Biological Chemistry 2009;284:4914–20.
Izumi K, Nakamura S, Nakano H, Shimura K, Sakagami Y, Oishi S, et al. Characterization of HIV-1 resistance to a fusion inhibitor, N36, derived from the gp41 amino-terminal heptad repeat. Antiviral Research 2010;87:179–86.
Kavlick MF, Wyvill K, Yarchoan R, Mitsuya H. Emergence of multi-dideoxynucleoside-resistant human immunodeficiency virus type 1 variants, viral sequence variation, and disease progression in patients receiving antiretroviral chemotherapy. Journal of Infectious Diseases 1998;177: 1506–13.
Kilby JM, Hopkins S, Venetta TM, DiMassimo B, Cloud GA, Lee JY, et al. Potent suppression of HIV-1 replication in humans by T-20, a peptide inhibitor of gp41-mediated virus entry. Nature Medicine 1998;4:1302–7.
Kosalaraksa P, Kavlick MF, Maroun V, Le R, Mitsuya H. Comparative fitness of multi-dideoxynucleoside-resistant human immunodeficiency virus type 1 (HIV-1) in an In vitro competitive HIV-1 replication assay. Jouranl of Virology 1999;73:5356–63.
Kuiken C, Foley B, Leitner T, Apetrei C, Hahn B, Mizrachi I, et al. HIV sequence compendium 2010. Los Alamos, NM: Los Alamos National Laboratory, Theoretical Biology and Biophysics; 2010.
Labrosse B, Labernardiere JL, Dam E, Trouplin V, Skrabal K, Clavel F, et al. Baseline susceptibility of primary human immunodeficiency virus type 1 to entry inhibitors. Journal of Virology 2003;77:1610–3.
Lalezari JP, Henry K, O'Hearn M, Montaner JS, Piliero PJ, Trottier B, et al. Enfuvirtide, an HIV-1 fusion inhibitor, for drug-resistant HIV infection in North and South America. New England Journal of Medicine 2003;348:2175–85.
Lazzarin A, Clotet B, Cooper D, Reynes J, Arasteh K, Nelson M, et al. Efficacy of enfuvirtide in patients infected with drug-resistant HIV-1 in Europe and Australia. New England Journal of Medicine 2003;348:2186–95.
Lohrengel S, Hermann F, Hagmann I, Oberwinkler H, Scrivano L, Hoffmann C, et al. Determinants of human immunodeficiency virus type 1 resistance to membrane-anchored gp41-derived peptides. Journal of Virology 2005;79:10237–46.
Loutfy MR, Raboud JM, Montaner JS, Antoniou T, Wynhoven B, Smaill F, et al. Assay of HIV gp41 amino acid sequence to identify baseline variation and mutation development in patients with virologic failure on enfuvirtide. Antiviral Research 2007;75:58–63.
Malashkevich VN, Chan DC, Chutkowski CT, Kim PS. Crystal structure of the simian immunodeficiency virus (SIV) gp41 core: conserved helical interactions underlie the broad inhibitory activity of gp41 peptides. Proceedings of the National Academy of Sciences of the United States of America 1998;95: 9134–9.
Melby T, Sista P, DeMasi R, Kirkland T, Roberts N, Salgo M, et al. Characterization of envelope glycoprotein gp41 genotype and phenotypic susceptibility to enfuvirtide at baseline and on treatment in the phase III clinical trials TORO-1 and TORO-2. AIDS Research and Human Retroviruses 2006;22:375–85.
Mink M, Mosier SM, Janumpalli S, Davison D, Jin L, Melby T, et al. Impact of human immunodeficiency virus type 1 gp41 amino acid substitutions selected during enfuvirtide treatment on gp41 binding and antiviral potency of enfuvirtide in vitro. Journal of Virology 2005;79:12447–54.
Nameki D, Kodama E, Ikeuchi M, Mabuchi N, Otaka A, Tamamura H, et al. Mutations conferring resistance to human immunodeficiency virus type 1 fusion inhibitors are restricted by gp41 and Rev-responsive element functions. Journal of Virology 2005;79:764–70.
Nishikawa H, Nakamura S, Kodama E, Ito S, Kajiwara K, Izumi K, et al. Electrostatically constrained alpha-helical peptide inhibits replication of HIV-1 resistant to enfuvirtide. International Journal of Biochemistry and Cell Biology 2009;41:891–9.
Oishi S, Ito S, Nishikawa H, Watanabe K, Tanaka M, Ohno H, et al. Design of a novel HIV-1 fusion inhibitor that displays a minimal interface for binding affinity. Journal of Medicinal Chemistry 2008;51:388–91.
Oliveira AC, Martins AN, Pires AF, Arruda MB, Tanuri A, Pereira HS, et al. Enfuvirtide (T-20) resistance-related mutations in HIV type 1 subtypes B, C, and F isolates from Brazilian patients failing HAART. AIDS Research and Human Retroviruses 2009;25:193–8.
Otaka A, Nakamura M, Nameki D, Kodama E, Uchiyama S, Nakamura S, et al. Remodeling of gp41-C34 peptide leads to highly effective inhibitors of the fusion of HIV-1 with target cells. Angewandte Chemie International Edition in English 2002;41:2937–40.
Reeves JD, Gallo SA, Ahmad N, Miamidian JL, Harvey PE, Sharron M, et al. Sensitivity of HIV-1 to entry inhibitors correlates with envelope/coreceptor affinity, receptor density, and fusion kinetics. Proceedings of the National Academy of Sciences of the United States of America 2002;99:16249–54.
Shimura K, Nameki D, Kajiwara K, Watanabe K, Sakagami Y, Oishi S, et al. Resistance profiles of novel electrostatically constrained HIV-1 fusion inhibitors. Journal of Biological Chemistry 2010;285:39471–80.
Shirasaka T, Kavlick MF, Ueno T, Gao WY, Kojima E, Alcaide ML, Chokekijchai S, Roy BM, Arnold E, Yarchoan R, et al. Emergence of human immunodeficiency virus type 1 variants with resistance to multiple dideoxynucleosides in patients receiving therapy with dideoxynucleosides. Proceedings of the National Academy of Sciences of the United States of America 1995;92:2398–402.
Svicher V, Aquaro S, D'Arrigo R, Artese A, Dimonte S, Alcaro S, et al. Specific enfuvirtide-associated mutational pathways in HIV-1 Gp41 are significantly correlated with an increase in CD4(+) cell count, despite virological failure. Journal of Infectious Diseases 2008;197:1408–18.
Tolstrup M, Selzer-Plon J, Laursen AL, Bertelsen L, Gerstoft J, Duch M, et al. Full fusion competence rescue of the enfuvirtide resistant HIV-1 gp41 genotype (43D) by a prevalent polymorphism (137 K). AIDS 2007;21:519–21.
Ueno M, Kodama EN, Shimura K, Sakurai Y, Kajiwara K, Sakagami Y, et al. Synonymous mutations in stem-loop III of Rev responsive elements enhance HIV-1 replication impaired by primary mutations for resistance to enfuvirtide. Antiviral Research 2009;82:67–72.
Watabe T, Terakawa Y, Watanabe K, Ohno H, Nakano H, Nakatsu T, et al. X-ray crystallographic study of an HIV-1 fusion inhibitor with the gp41 S138A substitution. Journal of Molecular Biology 2009;392:657–65.
Welch BD, VanDemark AP, Heroux A, Hill CP, Kay MS. Potent D-peptide inhibitors of HIV-1 entry. Proceedings of the National Academy of Sciences of the United States of America 2007;104:16828–33.
Xu L, Pozniak A, Wildfire A, Stanfield-Oakley SA, Mosier SM, Ratcliffe D, et al. Emergence and evolution of enfuvirtide resistance following long-term therapy involves heptad repeat 2 mutations within gp41. Antimicrobial Agents and Chemotherapy 2005;49:1113–9.

JVI
Journals.ASM.org

Comprehensive *In Vitro* Analysis of Simian Retrovirus Type 4 Susceptibility to Antiretroviral Agents

Hiroaki Togami,[a] Kazuya Shimura,[a] Munehiro Okamoto,[b] Rokusuke Yoshikawa,[c] Takayuki Miyazawa,[c] Masao Matsuoka[a]

Laboratory of Virus Control, Institute for Virus Research, Kyoto University, Kyoto, Japan[a]; Section of Wildlife Diversity, Center for Human Evolution Modeling Research, Primate Research Institute, Kyoto University, Inuyama, Japan[b]; Laboratory of Signal Transduction, Institute for Virus Research, Kyoto University, Kyoto, Japan[c]

Simian retrovirus type 4 (SRV-4), a simian type D retrovirus, naturally infects cynomolgus monkeys, usually without apparent symptoms. However, some infected monkeys presented with an immunosuppressive syndrome resembling that induced by simian immunodeficiency virus infection. Antiretrovirals with inhibitory activity against SRV-4 are considered to be promising agents to combat SRV-4 infection. However, although some antiretrovirals have been reported to have inhibitory activity against SRV-1 and SRV-2, inhibitors with anti-SRV-4 activity have not yet been studied. In this study, we identified antiretroviral agents with anti-SRV-4 activity from a panel of anti-human immunodeficiency virus (HIV) drugs using a robust *in vitro* luciferase reporter assay. Among these, two HIV reverse transcriptase inhibitors, zidovudine (AZT) and tenofovir disoproxil fumarate (TDF), potently inhibited SRV-4 infection within a submicromolar to nanomolar range, which was similar to or higher than the activities against HIV-1, Moloney murine leukemia virus, and feline immunodeficiency virus. In contrast, nonnucleoside reverse transcriptase inhibitors and protease inhibitors did not exhibit any activities against SRV-4. Although both AZT and TDF effectively inhibited cell-free SRV-4 transmission, they exhibited only partial inhibitory activities against cell-to-cell transmission. Importantly, one HIV integrase strand transfer inhibitor, raltegravir (RAL), potently inhibited single-round infection as well as cell-free and cell-to-cell SRV-4 transmission. These findings indicate that viral expansion routes impact the inhibitory activity of antiretrovirals against SRV-4, while only RAL is effective in suppressing both the initial SRV-4 infection and subsequent SRV-4 replication.

Simian type D retroviruses (SRV/Ds) are prevalent among wild and colony-born macaque monkeys, including *Macaca fascicularis* (cynomolgus) and *M. mulatta* (rhesus) (1–3). Although SRV/D infection is asymptomatic in most of these monkeys, mild immunosuppression accompanied by anemia, diarrhea, and splenomegaly has been observed in infected cynomolgus monkeys (3, 4). Recently, Japanese macaques (*M. fuscata*) housed in the Primate Research Institute (PRI) of Kyoto University, Japan, died of a hemorrhagic syndrome with symptoms such as anorexia, pallor, and nasal hemorrhage (5). Extensive investigations revealed that this illness was caused by an infection with an SRV/D known as simian retrovirus type 4 (SRV-4) (5; M. Okamoto et al., unpublished data). SRV-4 has been reported to be distantly related to other SRV/Ds, including SRV-1, -2, -3, -5, -6, and -7; e.g., the previously isolated SRV-4 showed genome sequence similarities of 78, 76, and 74% to SRV-1, -2, and -3, respectively (6). Although there is more than 80% amino acid sequence identity between Gag, Prt, and Pol of SRV-4 and SRV-1, -2, or -3, the Env sequence of SRV-4 is relatively diverse (67 to 74%) compared to other SRV/Ds (6). Although SRV-4 asymptomatically infects cynomolgus monkeys (7), SRV-4 infection of Japanese macaques has not been reported to date. Because the cause of the high mortality observed only for SRV-4-infected Japanese monkeys at PRI remains unclear, it is important to study SRV-4 pathogenesis in Japanese monkeys and to develop a prevention/treatment strategy for controlling SRV-4 infection.

Human immunodeficiency virus (HIV) infection remains a significant threat to humans. Over 20 antiviral drugs have been approved for the treatment of HIV-1-infected individuals. Antiretroviral therapy (ART) can efficiently suppress viral load and enable the recovery of immune function in HIV-1-infected individuals. Some of these drugs suppress infections caused by other retroviruses, including murine leukemia virus (MLV) (8, 9), xenotropic murine leukemia-related retrovirus (XMRV) (10, 11), feline immunodeficiency virus (FIV) (12, 13), and human T-cell leukemia virus type 1 (HTLV-1) (14, 15), indicating that some anti-HIV drugs are widely active against several other retroviruses. There have been some reports on the anti-SRV/D activity of anti-HIV drugs. Tsai et al. reported that three nucleoside/nucleotide reverse transcriptase inhibitors (NRTIs), zidovudine (AZT), zalcitabine (ddC), and 2′,3′-deoxyadenosine (ddA), exhibited inhibitory activity against SRV-2 infection *in vitro* (16). Moreover, although ddC treatment induced no major change in viral titers in pigtailed monkeys (*M. nemestrina*) naturally infected with SRV-2, the prophylactic use of ddC blocked *de novo* SRV-2 infection in this species (17). Rosenblum et al. reported that anti-SRV-1 and anti-SRV-2 activities of several NRTIs were relatively comparable with anti-HIV-1 activity (18). Furthermore, elvitegravir (EVG) and raltegravir (RAL), which are HIV-1 integrase strand transfer inhibitors (INSTIs), efficiently block SRV-3 (also known as Mason-Pfizer monkey virus) infection at nanomolar concentrations (19). Thus, some NRTIs and INSTIs exhibit anti-SRV/D activity; however, whether these drugs are active against SRV-4 infection remains unclear.

In this study, we extensively evaluated the anti-SRV-4 activity of a series of anti-HIV inhibitors, including NRTIs, nonnucleo-

Received 16 November 2012 Accepted 25 January 2013
Published ahead of print 30 January 2013
Address correspondence to Kazuya Shimura, kshimura@virus.kyoto-u.ac.jp.

doi:10.1128/JVI.03208-12

side reverse transcriptase inhibitors (NNRTIs), an INSTI, and protease inhibitors (PIs), *in vitro* using single-round infection and multiround viral spread by cell-free and cell-to-cell transmission. Among the NRTIs tested, AZT and tenofovir disoproxil fumarate (TDF) efficiently blocked single-round infection and cell-free transmission of SRV-4, although they were less effective against cell-to-cell transmission. RAL, an INSTI, blocked single-round infection and cell-free transmission of SRV-4 within the nanomolar range, and notably, it was also effective against cell-to-cell SRV-4 transmission. These results indicate that AZT, TDF, and RAL are effective in blocking the initial SRV-4 infection, and particularly, RAL is the most promising drug for the control of SRV-4 replication.

MATERIALS AND METHODS

Antiviral agents. Didanosine (ddI) (NRTI), lamivudine (3TC) (NRTI), stavudine (d4T) (NRTI), ddC (NRTI), AZT (NRTI), and nelfinavir (NFV) (PI) were purchased from Sigma (St. Louis, MO). Efavirenz (EFV) (NNRTI), nevirapine (NVP) (NNRTI), and saquinavir (SQV) (PI) were purchased from Toronto Research Chemicals (Ontario, Canada). Emtricitabine (FTC) (NRTI), TDF (NRTI), darunavir (DRV) (PI), and RAL (INSTI) were obtained through the AIDS Research and Reference Reagent Program, National Institute of Allergy and Infectious Diseases (NIAID), National Institutes of Health (NIH).

Cells and viruses. TE671 (human rhabdomyosarcoma), 293T (human embryonic kidney), and 293T/SRV-4 (a persistently SRV-4-infected 293T cell line) cells, which have been established by the transfection of an SRV-4 infectious clone into 293T cells (Okamoto et al., unpublished), were grown in Dulbecco's modified Eagle's medium (DMEM). MT-2 cells (human T lymphocytes) were grown in RPMI 1640 medium. These media were supplemented with 10% fetal calf serum (FCS), 2 mM L-glutamine, 100 U/ml penicillin, and 50 μg/ml streptomycin. 293FT cells (Invitrogen, Carlsbad, CA) were cultured in DMEM supplemented with 0.5 mg/ml G418. Platinum-GP cells (Plat-GP; Cell Biolabs, San Diego, CA) were maintained in DMEM supplemented with 10 μg/ml blasticidin.

Concentrated SRV-4 was prepared as follows: 293T/SRV-4 cells (10^6 cells) were cultured in a T-75 flask. After 3 days, culture supernatants were recovered and filtered through a 0.45-μm membrane, followed by the addition of a 30% polyethylene glycol (PEG) solution and 1.2 M sodium chloride. The mixture was then incubated overnight at 4°C, followed by centrifugation at 3,000 rpm for 45 min at 4°C. The resultant pellet was resuspended in DMEM and used for assays immediately after titration.

Quantification of the proviral copy number. Viral RNA and genomic DNA were prepared from concentrated SRV-4 by using the QIAamp viral RNA minikit (Qiagen, Hilden, Germany) and from SRV-4-infected 293T cells by using DNAzol (Invitrogen), respectively. The viral copy number was quantified by using the One Step PrimeScript reverse transcriptase PCR (RT-PCR) kit (TaKaRa, Otsu, Japan) and the StepOnePlus real-time PCR system (Applied Biosystems, Foster City, CA) with a known copy number control. The primer sets and a probe used for SRV-4 amplification were described previously (20). PCR conditions were 5 min at 42°C, 10 s at 95°C, and 55 cycles of 5 s at 95°C and 34 s at 62°C.

VSV-G-pseudotyped luciferase expression vectors. An envelope-deleted SRV-4-based firefly luciferase expression vector, Δenv-SRV-4-luc (R. Yoshikawa et al., unpublished data), and a plasmid, pcDNA-VSV-G, encoding the vesicular stomatitis virus envelope glycoprotein (VSV-G) (provided by H. Miyoshi, Riken Bioresource Center, Tsukuba, Japan) were used to generate VSV-G-pseudotyped luciferase-expressing SRV-4. These plasmids were cotransfected into 293FT cells. After 48 h of transfection, culture supernatants were recovered, filtered through a 0.45-μm membrane, and stored at −80°C until use.

The VSV-G-pseudotyped luciferase-expressing HIV-1-based lentiviral vector was generated as reported previously (9). The Moloney MLV (MoMLV)-based retroviral vector was produced by cotransfection of the pDON-AI-2-luc plasmid, a firefly luciferase gene-containing pDON-AI-2 retroviral vector (TaKaRa) (provided by Y. Sakurai, Institute for Virus Research, Kyoto University, Kyoto, Japan), and pcDNA-VSV-G into a MoMLV-based packaging cell line, Plat-GP. The FIV-based lentiviral vector was prepared by cotransfection of a luciferase-encoding transfer vector, pCDF-luc-EF1-puro; a 34TF10-derived packaging vector, pFIV-34N (SBI System Biosciences, Mountain View, CA); and pcDNA-VSV-G into 293FT cells. All the recombinant viruses were collected and stored as mentioned above.

Evaluation of the anti-SRV-4 activities of NRTIs, NNRTIs, and an INSTI in single-round infection. To evaluate the inhibitory activities of anti-HIV drugs against VSV-G-pseudotyped luciferase-expressing SRV-4, HIV-1, MoMLV, and FIV, TE671 cells (10^4 cells/well) were plated onto white 96-well flat plates. After 24 h of incubation, the cells were infected with each virus in the presence of various concentrations of inhibitors. Similarly, 3×10^5 MT-2 cells were infected separately. Luciferase activity was determined by using the Bright-Glo luciferase assay system (Promega, Madison, WI) and a TriStar LB 941 multimode microplate reader (Berthold, Bad Wildbad, Germany) at 48 h postinfection. Cytotoxicity of the inhibitors was measured by using the 3-(4,5-dimethylthiazol-2-yl)-2,5-diphenyltetrazolium bromide (MTT) colorimetric assay, as described previously (9). Antiviral activity and cytotoxicity of the inhibitors are presented as the concentration that blocks viral infection by 50% (50% effective concentration [EC_{50}]) and the concentration that inhibits cell viability by 50% (50% cytotoxic concentration [CC_{50}]), respectively.

Evaluation of the inhibitory activity of PI against SRV-4 production. 293T/SRV-4 cells were washed three times with phosphate-buffered saline (PBS) and plated at a density of 2×10^5 cells/well onto a six-well culture plate in the presence of various concentrations of PIs. After 72 h of incubation, culture supernatants were collected and concentrated as described above. The resultant pellet was solubilized with lysis buffer supplied in the Reverse Transcriptase Assay, colorimetric (Roche, Mannheim, Germany), and RT activity was quantified to evaluate viral production.

Effects of AZT, TDF, and RAL on SRV-4 replication. To test cell-free SRV-4 infection, 293T cells were plated at a density of 2×10^5 cells/well onto a six-well plate and pretreated with inhibitors of approximately 10× EC_{50}s determined by the single-round luciferase assay (AZT [400 nM], TDF [10 nM], and RAL [150 nM]) or dimethyl sulfoxide (DMSO) as a control for 4 h. Following this, culture media were replaced with fresh medium containing identical concentrations of each inhibitor, and the cells were infected with concentrated (37.5-fold) replication-competent SRV-4 at a multiplicity of infection (MOI) of 2.0×10^6 copies/cell.

For cell-to-cell SRV-4 infection, SRV-4-free 293T cells (2×10^5 cells) were pretreated with inhibitors as described above for the cell-free infection assay. Following this, 293T/SRV-4 cells (4×10^3 cells; proviral copy number, $5 \times 10^{1.3}$ copies/cell) were cocultured in the presence of identical concentrations of inhibitors.

In both the experimental approaches, culture supernatants were collected and replenished with an equal volume of fresh medium containing the corresponding inhibitors on days 1, 3, and 5 postinfection/postcoculture. SRV-4 in each collected supernatant was concentrated, and RT activity was quantified to monitor viral replication.

Statistical analysis. Dunnett's test and the Bonferroni test were used to determine the statistical significance of anti-SRV-4 activity of inhibitors in single-round assays (Table 1) and of SRV-4 transmission in cell-free and cell-to-cell infection assays (Fig. 1), respectively.

Protein sequence alignment. Standard amino acid sequences of SRV-4 (GenBank accession number NC_014474.1), HIV-1 (accession number NC_001802.1), MoMLV (accession number NC_001501.1), and FIV (accession number NC_001482.1) were aligned by using the program Clustal W (21), as described previously (9). Residues associated with drug resistance in HIV-1, reported in the Stanford University HIV Drug Resistance Database (22), are also shown.

TABLE 1 Susceptibility of VSV-G-pseudotyped luciferase-expressing SRV-4 and related retroviruses/lentiviruses to NRTIs and an INSTI in single-round infection[a]

Target cell line and inhibitor	Mean EC_{50} ± SD (μM) (mean % inhibition ± SD)			
	HIV-1	SRV-4	MoMLV	FIV
TE671				
NRTIs				
Thymidine analogs				
AZT	0.018 ± 0.0074	0.042 ± 0.012*	0.019 ± 0.0043	0.029 ± 0.0035
d4T	0.40 ± 0.10	0.17 ± 0.039	3.7 ± 0.82**	0.52 ± 0.0055
Inosine analog				
ddI	10 ± 1.7	4.4 ± 1.3**	>10 (0)	19 ± 1.7**
Cytidine analogs				
ddC	5.6 ± 1.1	2.7 ± 0.13**	>10 (0)**	3.2 ± 0.50**
3TC	4.4 ± 0.75	3.9 ± 1.2	>10 (0)**	2.2 ± 0.50*
FTC	0.48 ± 0.15	0.50 ± 0.082	>10 (0)**	0.35 ± 0.030
Adenosine analog				
TDF	0.0043 ± 0.00058	0.00080 ± 0.00037**	0.0035 ± 0.0012	0.0015 ± 0.00076**
INSTI				
RAL	0.0031 ± 0.0015	0.015 ± 0.0065	0.0017 ± 0.00036	0.049 ± 0.00090*
MT-2				
NRTIs				
Thymidine analogs				
AZT	0.037 ± 0.014	0.11 ± 0.037	0.71 ± 0.36*	1.4 ± 0.40**
d4T	0.50 ± 0.13	2.3 ± 0.44	3.5 ± 0.61	21 ± 6.6**
Inosine analog				
ddI	3.4 ± 0.70	>10 (42 ± 4.4)*	>10 (0)*	16 ± 4.7**
Cytidine analogs				
ddC	7.2 ± 2.4	0.59 ± 0.45**	>10 (0)	3.5 ± 1.1*
3TC	2.8 ± 1.0	>10 (17 ± 3.3)**	>10 (0)**	1.1 ± 0.10**
FTC	0.52 ± 0.12	3.0 ± 0.40**	>10 (0)**	0.22 ± 0.12
Adenosine analog				
TDF	0.0071 ± 0.0018	0.0016 ± 0.00025**	0.0071 ± 0.00056	0.0039 ± 0.0021
INSTI				
RAL	0.0033 ± 0.0010	0.0024 ± 0.00068	0.00064 ± 0.00057	0.062 ± 0.032**

[a] Antiviral activities of NRTIs and an INSTI against VSV-G-pseudotyped SRV-4, HIV-1, MoMLV, and FIV were determined by using a luciferase assay. Data are shown as means and standard deviations obtained from three or more independent experiments, and statistical analyses were performed (*, $P < 0.05$; **, $P < 0.01$; not indicated, $P \geq 0.05$ [determined by Dunnett's test against control HIV-1]). EC_{50}s shown as >10 indicate that more than 10 μM drugs is required to block viral infection by 50%. In this case, percent inhibition of viral infection at 10 μM is shown in parentheses and is considered 10 μM for statistical analysis.

RESULTS

Anti-SRV-4 activity of HIV NRTIs in single-round infection. To date, there is no convenient assay system for evaluating the anti-SRV-4 activity of compounds; therefore, we first established a simple and quantitative assay system by employing VSV-G-pseudotyped luciferase-expressing SRV-4 as a model virus. The anti-SRV-4 activity of the test compounds was evaluated by using TE671 and MT-2 cells. TE671 cells, which are derived from human rhabdomyosarcoma, have frequently been used for infection experiments with several retroviruses, including SRVs (23). MT-2 cells, which are derived from human T lymphocytes, are also susceptible to some viruses, including HIV (24) and hepatitis C virus (25), and are routinely used for analysis of antiviral activity of inhibitors (9). Inhibitory activity against HIV-1 and FIV (lentiviruses) and MoMLV (gammaretrovirus) was also evaluated.

Some HIV NRTIs reportedly possess anti-SRV-1 and anti-SRV-2 activities (16, 18); therefore, we first evaluated the anti-SRV-4 activity of seven NRTIs which have been approved for the treatment of HIV-1-infected patients. When TE671 cells were used as targets, ddI, ddC, and 3TC exhibited weak anti-SRV-4 activities, with EC_{50}s within the micromolar range (EC_{50}, 2.7 to 4.4 μM), whereas d4T and FTC exhibited moderate anti-SRV-4 activities, with EC_{50}s within the submicromolar range (EC_{50}, 0.2 and 0.5 μM, respectively) (Table 1). Remarkably, AZT and TDF exhibited potent anti-SRV-4 activities, with EC_{50}s of 42 and 0.8 nM, respectively. In contrast, almost all the NRTIs showed higher EC_{50}s using MT-2 cells as targets than those using TE671 cells as targets (Table 1). However, AZT and TDF exerted potent anti-SRV-4 activities, with EC_{50}s of 110 and 1.6 nM, respectively, even in the less sensitive MT-2 cells. Notably, all the NRTIs tested in this study exhibited no cytotoxicity against both cell types up to 100 μM, indicating that the observed anti-SRV-4 activity was not because of cell damage (data not shown).

One possible explanation for the difference in drug susceptibility between TE671 and MT-2 cells would be the different phosphorylation efficacies of NRTIs, which require sequential phosphorylations by cellular kinases to reach the active form (26, 27). To confirm this, we next evaluated anti-HIV-1, anti-FIV, and an-

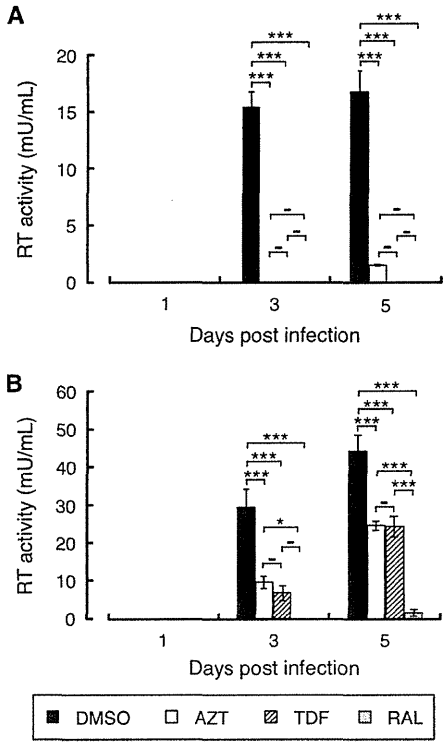

FIG 1 Effects of AZT, TDF, and RAL on SRV-4 replication. Anti-SRV-4 activities of AZT, TDF, and RAL were evaluated in cell-free transmission (A) and cell-to-cell transmission (B) models. SRV-4-free 293T cells were treated with AZT (400 nM), TDF (10 nM), RAL (150 nM), or vehicle (DMSO). After 4 h, culture media were replaced with fresh medium containing identical concentrations of each drug with replication-competent SRV-4 (A) or with SRV-4-infected 293T cells at a ratio of uninfected to infected cells of 50:1 (B). Culture supernatants were periodically collected, and SRV-4 was concentrated. The viral pellet was lysed, and reverse transcriptase activity derived from SRV-4 was quantified with a standard of known activity to monitor viral production. Data are shown as means and standard deviations obtained from three independent experiments. *, $P < 0.05$; **, $P < 0.01$; ***, $P < 0.001$; −, $P \geq 0.05$ (determined by the Bonferroni test).

ti-MoMLV activities using the same assay system, in which TE671 or MT-2 cells were infected with VSV-G-pseudotyped luciferase-expressing HIV-1- or FIV-based lentiviral vectors or MoMLV-based retroviral vectors in the presence of various concentrations of inhibitors. HIV-1 infection was blocked by all the tested NRTIs to various extents (Table 1). Among these, AZT and TDF exhibited potent activities against SRV-4 and MoMLV infections, while d4T was less active than AZT (Table 1). In FIV infection, AZT and d4T were active within the submicromolar range only in TE671 cells; however, TDF exhibited potent anti-FIV activity in both cell types (Table 1). Importantly, variation of EC_{50}s of NRTIs against HIV-1 was minimum between both target cell types (0.3- to 2.1-fold change in EC_{50}s measured with TE671 and MT-2 cells), suggesting that cell-derived factors are not a major cause of target cell-based differences in anti-SRV-4 activity.

Taken together, these findings indicate that HIV NRTIs have inhibitory activity against SRV-4 infection to various extents. Among these, AZT showed preferential anti-SRV-4 activity, a trend different from that previously observed against SRV-1 and SRV-2 (18). In addition, TDF exhibited the most potent anti-SRV-4 activity in the single-round infection assay.

Inhibitory effect of HIV-1 NNRTIs on SRV-4 infection. HIV-1 NNRTIs, including NVP and EFV, efficiently suppress HIV-1 infection by inhibiting HIV-1 RT activity by binding to a hydrophobic pocket near the RT polymerase active site (28, 29). In the present study, EFV showed slight cytotoxicity, with CC_{50} values of 57 and 48 μM in TE671 and MT-2 cells, respectively. However, both NVP and EFV potently inhibited HIV-1 infection, with EC_{50}s within the nanomolar to subnanomolar range (0.57 to 82 nM) in both cell types. In contrast, NVP and EFV were completely inactive against SRV-4 infection as well as against MoMLV and FIV infections, even at 10 μM. These results correlate well with the impressive narrow spectrum of NNRTI activity; i.e., NNRTIs are active against HIV-1 but not against HIV-2 and other retroviruses (11, 30–32).

Inhibitory activity of an HIV INSTI against SRV-4 infection. We next evaluated the inhibitory effect of RAL, the first INSTI approved for clinical use, on SRV-4 infection. RAL has potent anti-HIV-1 activity in addition to a broad antiviral spectrum including simian immunodeficiency virus (SIV) (33), MLV (34), XMRV (11), and SRV-3 (19). We also observed that RAL inhibited HIV-1 and MoMLV infections (Table 1). FIV was less susceptible to RAL than HIV-1 and MoMLV, although the RAL EC_{50} against FIV was at the nanomolar level. Most importantly, SRV-4 infection was potently inhibited by RAL within a nanomolar concentration (Table 1). We previously observed that EVG, a new INSTI contained within a recently approved anti-HIV drug, was active against not only HIV but also MoMLV and SIV (9), indicating that INSTIs are a preferential class of inhibitors for a wide range of retroviral infections. We report for the first time the potential blockage of SRV-4 infection by RAL without cytotoxicity.

Effect of HIV PIs on SRV-4 production. We then evaluated the inhibitory activity of PIs against SRV-4 replication. It is impossible to evaluate the anti-SRV-4 activity of PIs with the replication-deficient SRV-4 used to evaluate the inhibitory activities of NRTIs, NNRTIs, and an INSTI. To overcome this limitation, we evaluated persistently SRV-4-infected cells, in which the production of progeny infectious virions from SRV-4-infected 293T cells was monitored in the presence of various concentrations of PIs. Viruses released into culture supernatants were quantified by virion-derived RT activity.

First, we measured the cytotoxicity of three PIs (NFV, SQV, and DRV) against 293T cells. Although DRV showed no cytotoxicity up to 100 μM, NFV and SQV decreased cell viability, with CC_{50} values of 22 and 28 μM, respectively. To exclude a cell toxicity-based reduction in viral production, we used 0.1 and 1 μM concentrations of PIs in this study, which are sufficiently high to exert anti-HIV-1 activity (11, 35, 36). However, none of the PIs inhibited late-phase SRV-4 replication steps even at 1 μM (data not shown), indicating that SRV-4 is intrinsically less susceptible to PIs.

Effects of AZT, TDF, and RAL on SRV-4 replication. As observed in the early part of this study, two NRTIs (AZT and TDF) and one INSTI (RAL) efficiently inhibited replication-deficient SRV-4 infection in a single-cycle luciferase assay. To further elucidate the anti-SRV-4 property of these inhibitors, we assessed their effect on SRV-4 replication.

To precisely evaluate the inhibitory activity against SRV-4 replication, we distinguished the SRV-4 replication pattern into two viral expansion pathways: cell-free and cell-to-cell transmission. In the cell-free model, SRV-4-free 293T cells were infected with

cell-free SRV-4 in the presence of inhibitors, and further viral expansion was monitored by virus-derived RT activity. In contrast, SRV-4-infected 293T cells were used as the source of infection for cell-to-cell transmission.

We observed that in the cell-free model, SRV-4 efficiently infected 293T cells and reached the maximum level at 3 days postinfection (Fig. 1A). Similarly, viral expansion through *de novo* SRV-4 transmission was observed in the cell-to-cell model (Fig. 1B). However, SRV-4 expanded more efficiently through the cell-to-cell mechanism than through the cell-free mechanism, as judged by the 2- to 3-fold-higher RT activity observed in the cell-to-cell model at 5 days postinfection, indicating that cell-derived SRV-4 is a favorable source of SRV-4. Under these conditions, the 10-fold-higher EC_{50}s of AZT, TDF, and RAL, previously measured in single-round infection assays, completely inhibited cell-free SRV-4 infection up to 3 days (Fig. 1A). However, on day 5, only 7% of the viral production was observed in the presence of AZT, whereas TDF and RAL still almost completely blocked SRV-4 expansion. This tendency was well correlated with the antiviral activity measured during the single-round SRV-4 infection (Table 1). In contrast, when cell-associated SRV-4 was used as the infectious source, inhibitory activities of AZT and TDF were only partial; therefore, *de novo* SRV-4 transmission was ongoing at 3 and 5 days postinfection (Fig. 1B). Notably, we sequenced the RT regions of the proviral DNA at the end of this study, and no changes from the original SRV-4 were observed (data not shown). Thus, drug resistance was not associated with insufficient activity. However, only 3% to 5% of viral replication was observed in the presence of RAL on day 5 ($P < 0.001$, compared to AZT and TDF), indicating that RAL potently inhibited SRV-4 replication; therefore, it should be highly effective in controlling SRV-4 infection and replication.

DISCUSSION

To date, several SRV serotypes have been identified, and their distributions in monkeys have been revealed (1–3, 37–41). For example, SRV-4 and SRV-5 infect cynomolgus and rhesus monkeys, respectively, while the Japanese monkey is not a natural host of these SRVs (7, 42). However, the recent outbreak of SRV-4 at PRI revealed that Japanese monkeys are susceptible to SRV-4 (5), since fatal disease could be induced in some of them (43) (Okamoto et al., unpublished). These epidemics reflect the necessity for effective drugs against SRV-4 infection. In addition, human SRV infection has been reported, although no associated diseases have been identified (44). This finding also suggests that the identification of anti-SRV drugs is important to prevent the entry of these viruses into the human population.

Among the identified SRVs, the inhibitory activity of anti-HIV drugs against SRV-1 and SRV-2 has been relatively well analyzed. In these studies, the evaluation of anti-SRV activity was performed by time-consuming, cost-intensive, and hazardous procedures, e.g., using wild-type SRVs and infected monkeys (17, 18). In the present study, we used a VSV-G-pseudotyped luciferase reporter SRV-4 to screen inhibitors with anti-SRV-4 activity from a panel of clinically approved anti-HIV drugs. In this system, the luciferase reporter gene enabled sensitive and rapid evaluation. Moreover, replacement of the intrinsic envelope with VSV-G avoids the restriction of target cell tropism, thereby enabling the direct comparison of antiviral activity with other viruses in the same cells. Using this assay system, we reported for the first time that two anti-HIV NRTIs (AZT and TDF) and one INSTI (RAL) efficiently inhibited SRV-4 infection. The tendency for drug susceptibility of SRV-4 is different from that of SRV-1 and SRV-2, as reported in a previous study in which SRV-1 and SRV-2 infections were more potently inhibited by ddC than by AZT, 3TC, and d4T (18). Reportedly, SRV-4 is genetically distinct from SRV-1 and SRV-2 (3), suggesting that this intrinsic diversity reflects drug susceptibility.

Among the NRTIs tested, AZT and TDF exhibited potent anti-SRV-4 activities in single-round infection and cell-free viral transmission and also inhibited HIV-1, MoMLV, and FIV infections to various extents. However, the inhibitory activities of some NRTIs, particularly the thymidine analogs AZT and d4T, against SRV-4, MoMLV, and FIV infections were markedly (>10-fold) varied between TE671 and MT-2 cells (Table 1). A similar variation was previously reported for several viruses (18, 45). Major factors accounting for the different sensitivities of viruses to NRTIs in different target cells include the endogenous levels of some kinases as well as the levels of the intracellular pool of nucleotides (45–47). Moreover, although HIV-1 preferentially infects lymphoid cells, SRV infects a wide variety of cells, including not only $CD4^+$, $CD8^+$, and B cells *in vivo* but also lung fibroblast and kidney cells of monkeys *in vitro* (48). It is likely that the nature of the virus and assay conditions affects the susceptibility of SRV-4 to NRTIs in different cells, although further analyses are required to completely elucidate this phenomenon. TDF preferentially inhibited all the tested retroviruses. All the nucleoside-type RT inhibitors required three sequential phosphorylations, whereas TDF requires only a two-step phosphorylation to be active (49, 50), suggesting that this kinetic advantage reflects potent antiviral properties.

To gain deeper insights into the drug susceptibility of SRV-4, amino acid sequences of regions corresponding to the RT-polymerase domain (residues 63 to 234 of HIV-1) and the integrase catalytic core domain (IN-CCD) (residues 50 to 212) were compared with those of HIV-1, MoMLV, and FIV (Fig. 2). Because genotypic studies to elucidate drug susceptibility based on amino acid changes have been extensively performed for HIV-1 (22, 51, 52), we applied those observations to genotypic analysis of SRV-4. Overall, we confirmed that some amino acid residues in SRV-4 are identical to reported mutations affecting drug susceptibility in HIV-1. For example, HIV-1 RT mutations at positions 41, 67, 70, 210, 215, and 219, known as thymidine analog mutations (TAMs), are frequently observed in AZT and D4T resistance (52–54). In SRV-4 RT, some residues corresponding to TAMs differ from those of wild-type HIV-1 (Fig. 2A), although they must not be involved in drug susceptibility of SRV-4, since AZT and d4T inhibited SRV-4 infection at a similar or superior level compared to HIV-1 infection. In addition, although mutations at Q151 in the LPQG motif and M184 in the YMDD motif are involved in higher-level resistance to some NRTIs (55–57), these motifs are completely conserved in SRV-4 RT. In contrast, MoMLV showed complete insensitivity to certain NRTIs, including 3TC, at 10 μM (Table 1), in agreement with previous reports (8, 18). Taken together, as apparent from genotypic analysis of SRV-4 RT, AZT and TDF are thought to be potent therapeutic agents for the inhibition and control of SRV-4.

RAL, an HIV INSTI, showed potent inhibitory activity against SRV-4 infection as well as against HIV-1, MoMLV, and FIV infections. HIV-1 acquires high-level RAL resistance by mutations such as Q148H/R/K and N155H (52, 58). Although SRV-4 IN

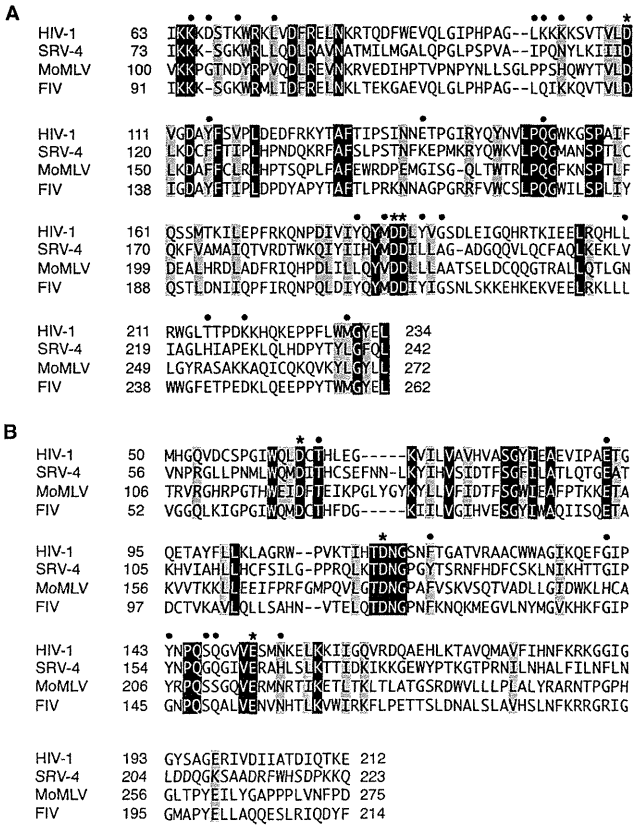

FIG 2 Protein sequence alignments of RT and IN. Reference amino acid sequences of SRV-4 (GenBank accession number NC_014474.1), HIV-1 (accession number NC_001802.1), MoMLV (accession number NC_001501.1), and FIV (accession number NC_001482.1) were aligned by using the program Clustal W, and the regions corresponding to the RT-polymerase domain (residues 63 to 234) (A) and the IN catalytic core domain (residues 50 to 212) (B) of HIV-1 are shown. The amino acid numbering of SRV-4 IN is based on that of SRV-3 (68). Absolutely conserved residues and conserved substitutions are shown in black and gray boxes, respectively. For symbols above the sequences, closed circles indicate residues associated with drug resistance for HIV-1, and asterisks indicate catalytic residues.

contains H166, which corresponds to N155 in HIV-1 (Fig. 2B), SRV-4 retained susceptibility within levels similar to those of wild-type HIV-1 (Table 1). Reportedly, SRV-3 also contains amino acids corresponding to N155H and F121Y, which are other INSTI resistance mutations; however, SRV-3 shows complete susceptibility to RAL (19). In contrast, bovine immunodeficiency virus (BIV) reportedly showed 23-fold resistance to RAL compared to wild-type HIV-1, although BIV contains a histidine (H) residue at the position corresponding to N155 (19), as seen in SRV-4, indicating that N155H is not a determinant of RAL susceptibility in retroviruses other than HIV. Although in the present study, FIV showed less susceptibility to RAL than the other retroviruses/lentiviruses tested (Table 1), FIV does not contain major INSTI resistance mutations. However, one distinct difference was observed: FIV IN carries G145, whereas it corresponds to Y143 in HIV-1 (Fig. 2B). The Y143G mutation has rarely been observed in RAL-treated patients (59); therefore, the precise effect of this mutation on RAL resistance remains unclear. However, it was speculated that that the Y143G mutation lacks the interaction with RAL (19), and interestingly, Y143G reportedly affects proviral formation (60), although this is apparent in nondividing cells (61), likely suggesting that FIV IN G145 affects susceptibility of FIV not only to INSTIs but also to NRTIs.

To expand viral infection *in vitro* and *in vivo*, viruses utilize two main pathways: cell-free and cell-to-cell transmission. However, the transmission pathway depends on the nature of the viruses. For example, cell-free HIV-1 efficiently infects $CD4^+$ T cells and also spreads in a cell-to-cell manner, whereas HTLV-1 transmits exclusively by a cell-to-cell pathway (62–66). In the present study, we compared the inhibitory activities of some inhibitors against SRV-4 replication in both cell-free and cell-to-cell transmission. We observed that although AZT and TDF could almost completely block cell-free SRV-4 transmission, they showed only marginal effects on cell-to-cell SRV-4 transmission (Fig. 1). In contrast, RAL completely suppressed SRV-4 replication in both cell-free and cell-to-cell transmission. These results indicate that a favorable pathway is intrinsically present in anti-HIV-1 drugs; AZT and TDF preferentially block cell-free infection, whereas RAL is active in both the pathways. A similar observation was reported for HIV-1, in which tenofovir preferentially suppressed cell-free transmission compared with cell-to-cell transmission (67). These observations may highlight the importance of the kinetics of viral replication and drug activation because AZT and TDF require tri- and diphosphorylation, respectively, to become active metabolites, whereas RAL does not require any modification to exert its antiviral activity. In addition, it is likely that the kinetics of SRV-4 replication steps, including reverse transcription and integration, vary between cell-free and cell-to-cell transmission, as seen for HIV-1; this may be another determinant of viral transmission pathway-dependent anti-SRV-4 activities.

Taken together, the present study demonstrated that AZT, TDF, and RAL potently inhibited SRV-4 infection. These inhibitors suppressed single-round infection and cell-free virus transmission of SRV-4; however, cell-to-cell transmission was blocked only by RAL. To effectively control SRV-4 infection and maintain a minimum risk of the emergence of drug resistance, a combination therapy of drugs such as ART in HIV-1 infection is important.

ACKNOWLEDGMENTS

We thank H. Miyoshi and Y. Sakurai for providing lentiviral vectors and the pDON-AI-2-luc vector, respectively. The following reagents were obtained through the NIH AIDS Research and Reference Reagent Program, Division of AIDS, NIAID, NIH: emtricitabine, tenofovir disoproxil fumarate, darunavir (from Tibotec, Inc.), and raltegravir (from Merck & Company, Inc.).

This work was supported in part by a JSPS KAKENHI grant-in-aid for young scientists (B) to K.S. (grant number 24791021) and a grant-in-aid for scientific research (B) to M.O. (grant number 24300153).

REFERENCES

1. Daniel MD, King NW, Letvin NL, Hunt RD, Sehgal PK, Desrosiers RC. 1984. A new type D retrovirus isolated from macaques with an immunodeficiency syndrome. Science 223:602–605.
2. Marx PA, Maul DH, Osborn KG, Lerche NW, Moody P, Lowenstine LJ, Henrickson RV, Arthur LO, Gilden RV, Gravell M. 1984. Simian AIDS: isolation of a type D retrovirus and transmission of the disease. Science 223:1083–1086.
3. Montiel NA. 2010. An updated review of simian betaretrovirus (SRV) in macaque hosts. J. Med. Primatol. 39:303–314.
4. Henrickson RV, Maul DH, Lerche NW, Osborn KG, Lowenstine LJ, Prahalada S, Sever JL, Madden DL, Gardner MB. 1984. Clinical features

of simian acquired immunodeficiency syndrome (SAIDS) in rhesus monkeys. Lab. Anim. Sci. 34:140–145.
5. CDC-KUPRI. 2010. Information of hemorrhagic syndrome of Japanese macaques (provisional designation). Primate Res. 26:69–71.
6. Zao CL, Armstrong K, Tomanek L, Cooke A, Berger R, Estep JS, Marx PA, Trask JS, Smith DG, Yee JL, Lerche NW. 2010. The complete genome and genetic characteristics of SRV-4 isolated from cynomolgus monkeys (Macaca fascicularis). Virology 405:390–396.
7. Zao CL, Ward JA, Tomanek L, Cooke A, Berger R, Armstrong K. 2011. Virological and serological characterization of SRV-4 infection in cynomolgus macaques. Arch. Virol. 156:2053–2056.
8. Powell SK, Artlip M, Kaloss M, Brazinski S, Lyons R, McGarrity GJ, Otto E. 1999. Efficacy of antiretroviral agents against murine replication-competent retrovirus infection in human cells. J. Virol. 73:8813–8816.
9. Shimura K, Kodama E, Sakagami Y, Matsuzaki Y, Watanabe W, Yamataka K, Watanabe Y, Ohata Y, Doi S, Sato M, Kano M, Ikeda S, Matsuoka M. 2008. Broad antiretroviral activity and resistance profile of the novel human immunodeficiency virus integrase inhibitor elvitegravir (JTK-303/GS-9137). J. Virol. 82:764–774.
10. Sakuma R, Sakuma T, Ohmine S, Silverman RH, Ikeda Y. 2010. Xenotropic murine leukemia virus-related virus is susceptible to AZT. Virology 397:1–6.
11. Smith RA, Gottlieb GS, Miller AD. 2010. Susceptibility of the human retrovirus XMRV to antiretroviral inhibitors. Retrovirology 7:70. doi:10.1186/1742-4690-7-70.
12. Zhu YQ, Remington KM, North TW. 1996. Mutants of feline immunodeficiency virus resistant to 2′,3′-dideoxy-2′,3′-didehydrothymidine. Antimicrob. Agents Chemother. 40:1983–1987.
13. North TW, North GL, Pedersen NC. 1989. Feline immunodeficiency virus, a model for reverse transcriptase-targeted chemotherapy for acquired immune deficiency syndrome. Antimicrob. Agents Chemother. 33:915–919.
14. Matsushita S, Mitsuya H, Reitz MS, Broder S. 1987. Pharmacological inhibition of in vitro infectivity of human T lymphotropic virus type I. J. Clin. Invest. 80:394–400.
15. Miyazato P, Yasunaga J, Taniguchi Y, Koyanagi Y, Mitsuya H, Matsuoka M. 2006. De novo human T-cell leukemia virus type 1 infection of human lymphocytes in NOD-SCID, common gamma-chain knockout mice. J. Virol. 80:10683–10691.
16. Tsai CC, Follis KE, Benveniste RE. 1988. Antiviral effects of 3′-azido-3′-deoxythymidine, 2′,3′-dideoxycytidine, and 2′,3′-dideoxyadenosine against simian acquired immunodeficiency syndrome-associated type D retrovirus in vitro. AIDS Res. Hum. Retroviruses 4:359–368.
17. Tsai CC, Follis KE, Yarnall M, Blakley GA. 1989. Toxicity and efficacy of 2′,3′-dideoxycytidine in clinical trials of pigtailed macaques infected with simian retrovirus type 2. Antimicrob. Agents Chemother. 33:1908–1914.
18. Rosenblum LL, Patton G, Grigg AR, Frater AJ, Cain D, Erlwein O, Hill CL, Clarke JR, McClure MO. 2001. Differential susceptibility of retroviruses to nucleoside analogues. Antivir. Chem. Chemother. 12:91–97.
19. Koh Y, Matreyek KA, Engelman A. 2011. Differential sensitivities of retroviruses to integrase strand transfer inhibitors. J. Virol. 85:3677–3682.
20. White JA, Todd PA, Rosenthal AN, Yee JL, Grant R, Lerche NW. 2009. Development of a generic real-time PCR assay for simultaneous detection of proviral DNA of simian betaretrovirus serotypes 1, 2, 3, 4 and 5 and secondary uniplex assays for specific serotype identification. J. Virol. Methods 162:148–154.
21. Thompson JD, Higgins DG, Gibson TJ. 1994. CLUSTAL W: improving the sensitivity of progressive multiple sequence alignment through sequence weighting, position-specific gap penalties and weight matrix choice. Nucleic Acids Res. 22:4673–4680.
22. Rhee SY, Gonzales MJ, Kantor R, Betts BJ, Ravela J, Shafer RW. 2003. Human immunodeficiency virus reverse transcriptase and protease sequence database. Nucleic Acids Res. 31:298–303.
23. Tailor CS, Nouri A, Zhao Y, Takeuchi Y, Kabat D. 1999. A sodium-dependent neutral-amino-acid transporter mediates infections of feline and baboon endogenous retroviruses and simian type D retroviruses. J. Virol. 73:4470–4474.
24. Harada S, Koyanagi Y, Yamamoto N. 1985. Infection of HTLV-III/LAV in HTLV-I-carrying cells MT-2 and MT-4 and application in a plaque assay. Science 229:563–566.
25. Kato N, Nakazawa T, Mizutani T, Shimotohno K. 1995. Susceptibility of human T-lymphotropic virus type I infected cell line MT-2 to hepatitis C virus infection. Biochem. Biophys. Res. Commun. 206:863–869.
26. Cihlar T, Ray AS. 2010. Nucleoside and nucleotide HIV reverse transcriptase inhibitors: 25 years after zidovudine. Antiviral Res. 85:39–58.
27. Piliero PJ. 2004. Pharmacokinetic properties of nucleoside/nucleotide reverse transcriptase inhibitors. J. Acquir. Immune Defic. Syndr. 37(Suppl 1):S2–S12. http://download.bioon.com.cn/upload/201101/17/101159hswyecdhh77cw6xv.attach.pdf.
28. Ren J, Stammers DK. 2008. Structural basis for drug resistance mechanisms for non-nucleoside inhibitors of HIV reverse transcriptase. Virus Res. 134:157–170.
29. Huang H, Chopra R, Verdine GL, Harrison SC. 1998. Structure of a covalently trapped catalytic complex of HIV-1 reverse transcriptase: implications for drug resistance. Science 282:1669–1675.
30. Auwerx J, Esnouf R, De Clercq E, Balzarini J. 2004. Susceptibility of feline immunodeficiency virus/human immunodeficiency virus type 1 reverse transcriptase chimeras to non-nucleoside RT inhibitors. Mol. Pharmacol. 65:244–251.
31. Ren J, Bird LE, Chamberlain PP, Stewart-Jones GB, Stuart DI, Stammers DK. 2002. Structure of HIV-2 reverse transcriptase at 2.35-A resolution and the mechanism of resistance to non-nucleoside inhibitors. Proc. Natl. Acad. Sci. U. S. A. 99:14410–14415.
32. Witvrouw M, Pannecouque C, Switzer WM, Folks TM, De Clercq E, Heneine W. 2004. Susceptibility of HIV-2, SIV and SHIV to various anti-HIV-1 compounds: implications for treatment and postexposure prophylaxis. Antivir. Ther. 9:57–65.
33. Lewis MG, Norelli S, Collins M, Barreca ML, Iraci N, Chirullo B, Yalley-Ogunro J, Greenhouse J, Titti F, Garaci E, Savarino A. 2010. Response of a simian immunodeficiency virus (SIVmac251) to raltegravir: a basis for a new treatment for simian AIDS and an animal model for studying lentiviral persistence during antiretroviral therapy. Retrovirology 7:21. doi:10.1186/1742-4690-7-21.
34. Beck-Engeser GB, Eilat D, Harrer T, Jäck HM, Wabl M. 2009. Early onset of autoimmune disease by the retroviral integrase inhibitor raltegravir. Proc. Natl. Acad. Sci. U. S. A. 106:20865–20870.
35. Koh Y, Nakata H, Maeda K, Ogata H, Bilcer G, Devasamudram T, Kincaid JF, Boross P, Wang YF, Tie Y, Volarath P, Gaddis L, Harrison RW, Weber IT, Ghosh AK, Mitsuya H. 2003. Novel bis-tetrahydrofuranylurethane-containing nonpeptidic protease inhibitor (PI) UIC-94017 (TMC114) with potent activity against multi-PI-resistant human immunodeficiency virus in vitro. Antimicrob. Agents Chemother. 47:3123–3129.
36. Patick AK, Mo H, Markowitz M, Appelt K, Wu B, Musick L, Kalish V, Kaldor S, Reich S, Ho D, Webber S. 1996. Antiviral and resistance studies of AG1343, an orally bioavailable inhibitor of human immunodeficiency virus protease. Antimicrob. Agents Chemother. 40:292–297.
37. Hara M, Sata T, Kikuchi T, Nakajima N, Uda A, Fujimoto K, Baba T, Mukai R. 2005. Isolation and characterization of a new simian retrovirus type D subtype from monkeys at the Tsukuba Primate Center, Japan. Microbes Infect. 7:126–131.
38. Marx PA, Bryant ML, Osborn KG, Maul DH, Lerche NW, Lowenstine LJ, Kluge JD, Zaiss CP, Henrickson RV, Shiigi SM. 1985. Isolation of a new serotype of simian acquired immune deficiency syndrome type D retrovirus from Celebes black macaques (Macaca nigra) with immune deficiency and retroperitoneal fibromatosis. J. Virol. 56:571–578.
39. Nandi JS, Bhavalkar-Potdar V, Tikute S, Raut CG. 2000. A novel type D simian retrovirus naturally infecting the Indian Hanuman langur (Semnopithecus entellus). Virology 277:6–13.
40. Nandi JS, Tikute SA, Chhangani AK, Potdar VA, Tiwari-Mishra M, Ashtekar RA, Kumari J, Walimbe A, Mohnot SM. 2003. Natural infection by simian retrovirus-6 (SRV-6) in Hanuman langurs (Semnopithecus entellus) from two different geographical regions of India. Virology 311:192–201.
41. Nandi JS, Van Dooren S, Chhangani AK, Mohnot SM. 2006. New simian beta retroviruses from rhesus monkeys (Macaca mulatta) and langurs (Semnopithecus entellus) from Rajasthan, India. Virus Genes 33:107–116.
42. Li B, Axthelm MK, Machida CA. 2000. Simian retrovirus serogroup 5: partial gag-prt sequence and viral RNA distribution in an infected rhesus macaque. Virus Genes 21:241–248.
43. Cyranoski D. 2010. Japanese monkey deaths puzzle. Nature 466:302–303.
44. Lerche NW, Switzer WM, Yee JL, Shanmugam V, Rosenthal AN, Chapman LE, Folks TM, Heneine W. 2001. Evidence of infection with simian type D retrovirus in persons occupationally exposed to nonhuman primates. J. Virol. 75:1783–1789.

45. Dahlberg JE, Mitsuya H, Blam SB, Broder S, Aaronson SA. 1987. Broad spectrum antiretroviral activity of 2′,3′-dideoxynucleosides. Proc. Natl. Acad. Sci. U. S. A. 84:2469–2473.
46. Balzarini J. 2000. Effect of antimetabolite drugs of nucleotide metabolism on the anti-human immunodeficiency virus activity of nucleoside reverse transcriptase inhibitors. Pharmacol. Ther. 87:175–187.
47. Ray AS. 2005. Intracellular interactions between nucleos(t)ide inhibitors of HIV reverse transcriptase. AIDS Rev. 7:113–125.
48. Maul DH, Zaiss CP, MacKenzie MR, Shiigi SM, Marx PA, Gardner MB. 1988. Simian retrovirus D serogroup 1 has a broad cellular tropism for lymphoid and nonlymphoid cells. J. Virol. 62:1768–1773.
49. De Clercq E, Holý A. 2005. Acyclic nucleoside phosphonates: a key class of antiviral drugs. Nat. Rev. Drug Discov. 4:928–940.
50. De Clercq E. 2009. The history of antiretrovirals: key discoveries over the past 25 years. Rev. Med. Virol. 19:287–299.
51. Shafer RW. 2006. Rationale and uses of a public HIV drug-resistance database. J. Infect. Dis. 194(Suppl 1):S51–S58. doi:10.1086/505356.
52. Johnson VA, Calvez V, Günthard HF, Paredes R, Pillay D, Shafer R, Wensing AM, Richman DD. 2011. 2011 update of the drug resistance mutations in HIV-1. Top. Antivir. Med. 19:156–164.
53. Gao Q, Gu ZX, Parniak MA, Li XG, Wainberg MA. 1992. In vitro selection of variants of human immunodeficiency virus type 1 resistant to 3′-azido-3′-deoxythymidine and 2′,3′-dideoxyinosine. J. Virol. 66:12–19.
54. Lin PF, Samanta H, Rose RE, Patick AK, Trimble J, Bechtold CM, Revie DR, Khan NC, Federici ME, Li H. 1994. Genotypic and phenotypic analysis of human immunodeficiency virus type 1 isolates from patients on prolonged stavudine therapy. J. Infect. Dis. 170:1157–1164.
55. Quan Y, Gu Z, Li X, Liang C, Parniak MA, Wainberg MA. 1998. Endogenous reverse transcriptase assays reveal synergy between combinations of the M184V and other drug resistance-conferring mutations in interactions with nucleoside analog triphosphates. J. Mol. Biol. 277:237–247.
56. Shirasaka T, Kavlick MF, Ueno T, Gao WY, Kojima E, Alcaide ML, Chokekijchai S, Roy BM, Arnold E, Yarchoan R. 1995. Emergence of human immunodeficiency virus type 1 variants with resistance to multiple dideoxynucleosides in patients receiving therapy with dideoxynucleosides. Proc. Natl. Acad. Sci. U. S. A. 92:2398–2402.
57. Tisdale M, Kemp SD, Parry NR, Larder BA. 1993. Rapid in vitro selection of human immunodeficiency virus type 1 resistant to 3′-thiacytidine inhibitors due to a mutation in the YMDD region of reverse transcriptase. Proc. Natl. Acad. Sci. U. S. A. 90:5653–5656.
58. Fransen S, Gupta S, Danovich R, Hazuda D, Miller M, Witmer M, Petropoulos CJ, Huang W. 2009. Loss of raltegravir susceptibility by human immunodeficiency virus type 1 is conferred via multiple nonoverlapping genetic pathways. J. Virol. 83:11440–11446.
59. Canducci F, Sampaolo M, Marinozzi MC, Boeri E, Spagnuolo V, Galli A, Castagna A, Lazzarin A, Clementi M, Gianotti N. 2009. Dynamic patterns of human immunodeficiency virus type 1 integrase gene evolution in patients failing raltegravir-based salvage therapies. AIDS 23:455–460.
60. Ikeda T, Nishitsuji H, Zhou X, Nara N, Ohashi T, Kannagi M, Masuda T. 2004. Evaluation of the functional involvement of human immunodeficiency virus type 1 integrase in nuclear import of viral cDNA during acute infection. J. Virol. 78:11563–11573.
61. Tsurutani N, Kubo M, Maeda Y, Ohashi T, Yamamoto N, Kannagi M, Masuda T. 2000. Identification of critical amino acid residues in human immunodeficiency virus type 1 IN required for efficient proviral DNA formation at steps prior to integration in dividing and nondividing cells. J. Virol. 74:4795–4806.
62. Igakura T, Stinchcombe JC, Goon PK, Taylor GP, Weber JN, Griffiths GM, Tanaka Y, Osame M, Bangham CR. 2003. Spread of HTLV-I between lymphocytes by virus-induced polarization of the cytoskeleton. Science 299:1713–1716.
63. Jolly C, Kashefi K, Hollinshead M, Sattentau QJ. 2004. HIV-1 cell to cell transfer across an Env-induced, actin-dependent synapse. J. Exp. Med. 199:283–293.
64. Sattentau Q. 2008. Avoiding the void: cell-to-cell spread of human viruses. Nat. Rev. Microbiol. 6:815–826.
65. Pais-Correia AM, Sachse M, Guadagnini S, Robbiati V, Lasserre R, Gessain A, Gout O, Alcover A, Thoulouze MI. 2010. Biofilm-like extracellular viral assemblies mediate HTLV-1 cell-to-cell transmission at virological synapses. Nat. Med. 16:83–89.
66. Matsuoka M, Jeang KT. 2007. Human T-cell leukaemia virus type 1 (HTLV-1) infectivity and cellular transformation. Nat. Rev. Cancer 7:270–280.
67. Sigal A, Kim JT, Balazs AB, Dekel E, Mayo A, Milo R, Baltimore D. 2011. Cell-to-cell spread of HIV permits ongoing replication despite antiretroviral therapy. Nature 477:95–98.
68. Snásel J, Krejcík Z, Jencová V, Rosenberg I, Ruml T, Alexandratos J, Gustchina A, Pichová I. 2005. Integrase of Mason-Pfizer monkey virus. FEBS J. 272:203–216.

OPEN ACCESS Freely available online

PLoS one

Structural Dynamics of HIV-1 Envelope Gp120 Outer Domain with V3 Loop

Masaru Yokoyama[1]*, Satoshi Naganawa[2], Kazuhisa Yoshimura[3], Shuzo Matsushita[3], Hironori Sato[1]*

1 Laboratory of Viral Genomics, Pathogen Genomics Center, National Institute of Infectious Diseases, 4-7-1 Gakuen, Musashi Murayama-shi, Tokyo, Japan, **2** Department of Microbiology and Cell Biology, Tokyo Metropolitan Institute of Medical Science, 2-1-6 Kamikitazawa, Setagaya-ku, Tokyo, Japan, **3** Division of Clinical Retrovirology and Infectious Diseases, Center for AIDS Research, Kumamoto University, 2-2-1 Honjo, Kumamoto, Japan

Abstract

Background: The net charge of the hypervariable V3 loop on the HIV-1 envelope gp120 outer domain plays a key role in modulating viral phenotype. However, the molecular mechanisms underlying the modulation remain poorly understood.

Methodology/Principal Findings: By combining computational and experimental approaches, we examined how V3 net charge could influence the phenotype of the gp120 interaction surface. Molecular dynamics simulations of the identical gp120 outer domain, carrying a V3 loop with net charge of +3 or +7, showed that the V3 change alone could induce global changes in fluctuation and conformation of the loops involved in binding to CD4, coreceptor and antibodies. A neutralization study using the V3 recombinant HIV-1 infectious clones showed that the virus carrying the gp120 with +3 V3, but not with +7 V3, was resistant to neutralization by anti-CD4 binding site monoclonal antibodies. An information entropy study shows that otherwise variable surface of the gp120 outer domain, such as V3 and a region around the CD4 binding loop, are less heterogeneous in the gp120 subpopulation with +3 V3.

Conclusions/Significance: These results suggest that the HIV-1 gp120 V3 loop acts as an electrostatic modulator that influences the global structure and diversity of the interaction surface of the gp120 outer domain. Our findings will provide a novel structural basis to understand how HIV-1 adjusts relative replication fitness by V3 mutations.

Citation: Yokoyama M, Naganawa S, Yoshimura K, Matsushita S, Sato H (2012) Structural Dynamics of HIV-1 Envelope Gp120 Outer Domain with V3 Loop. PLoS ONE 7(5): e37530. doi:10.1371/journal.pone.0037530

Editor: John J. Rossi, Beckman Research Institute of the City of Hope, United States of America

Received February 21, 2012; **Accepted** April 20, 2012; **Published** May 18, 2012

Funding: This work was supported by grants-in-aid from the Ministry of Health, Labor and Welfare, Japan. The funders had no role in study design, data collection and analysis, decision to publish, or preparation of the manuscript.

Competing Interests: The authors have declared that no competing interests exist.

* E-mail: yokoyama@nih.go.jp (MY); hirosato@nih.go.jp (HS)

Introduction

The third variable (V3) element of the human immunodeficiency virus type 1 (HIV-1) envelope gp120 protein is usually composed of 35 amino acids. The element forms a protruding loop-like structure on the gp120 outer domain [1], is rich in basic amino acids, and has aromatic amino acids for the aromatic stacking interaction with proteins. The V3 loop participates in direct binding to the entry coreceptor [2] and constitutes the most critical determinant for the coreceptor use of HIV-1 [3,4,5,6]. In addition, the tip of V3 is highly immunogenic and contains neutralization epitopes for antibodies [7,8,9], although the epitopes can be inaccesible in the gp120 trimer on a virion of the HIV-1 primary isolates [10,11] or HIV-1 recombinants with less positively charged V3 [12,13]. Moreover, the V3 is reported to be the major determinant of HIV-1 sensitivity to neutralization by the soluble form of CD4 [14,15,16], a recombinant protein that binds to the cleft of the gp120 core [17]. Thus, the V3 loop plays a key role in modulating biological and immunological phenotypes of HIV-1. However, the molecular mechanisms underlying these modulations remain poorly understood.

It has been reported that the net charge of the V3 loop is tightly linked to the phenotype of HIV-1. The V3 loops of CCR5 tropic HIV-1s are usually less positively charged than those of CXCR4 tropic HIV-1s [18,19,20,21]. An increase in the V3 net charge can convert CCR5 tropic viruses into CXCR4 tropic viruses [4,22,23,24], and antibody resistant viruses into sensitive viruses [12,13]. Thus the V3 loop may be viewed as an electrostatic modulator of the structure of the gp120 interaction surface, an assumption that is largely unexamined.

Increasing evidence has indicated that the dynamics property of molecules in solution is critical for protein function and thus for many biological processes [25,26,27]. Molecular dynamic (MD) simulation is a powerful method that predicts the structural dynamics of biological molecules in solution, which is often difficult to analyze by experiments alone [28,29,30]. Recent advances in biomolecular simulation have rapidly improved the precision and application performance of this technique [28,29,30]. We have previously applied this technique to investigating the structural factors that regulate biological phenotype of viruses [13,31,32]. In this study, by combining MD simulations with antibody neutralization experiments and diversity analysis of the viral protein sequences, we studied a structural basis for the regulation of HIV-1 phenotype by V3 loop.

Results

Molecular dynamics simulation study

To address the potential role of the V3 net charge in modulating the structure and dynamics of the gp120 surface, we performed MD simulations of the identical gp120 outer domains carrying different V3 loops with net charges of +7 or +3 (Fig. 1A). The initial structures for the simulations were constructed by homology modeling using the crystal structure of HIV-1 gp120 containing an entire V3 loop as the template. Due to the perfect identity of the outer domain sequences of the V3 recombinant gp120s, the outer domain structures of the initial models for the MD simulations were identical before the simulations. The modeling targets in this study belong to HIV-1 subtype B and had a sequence similarity of about 87.3% to the modeling template. This similarity was high enough to construct high-accuracy models with an RMSD of ~1.5 Å for the main chain between the predicted and actual structures in the tested cases with homology models and x-ray crystal structures [33]. These initial models were lacking in V1/V2 loops and glycans on the gp120. The recombinant models are therefore suitable for exploring the potency of the structural regulation that is intrinsic to the V3 loop.

Using these models as the initial structures, we analyzed the structural dynamics of the gp120 outer domains in the absence of soluble CD4 by MD simulation. It was expected that the MD simulations would eliminate initial distortions in the template crystal structure, which could be generated during crystallization, and search for the most stable structures of unliganded gp120 outer domains at 1 atm at 310 K in water. The simulations showed that the same gp120 outer domains, carrying different V3 loops with net charges of +7 or +3, exhibited marked changes in conformations and fluctuations at several functional loops at 1 atm at 310 K in water (Figs. 1 and 2).

To quantitatively monitor the overall structural dynamics of the outer domain during MD simulation, the RMSDs between the initial model and models at given times of MD simulation were measured. The RMSD sharply increased soon after heating of the initial model and then gradually reached a near plateau after 10 ns of the MD simulations (Fig. 1B). The results suggested that most of the backbone heavy atoms of the outer domain reached a thermodynamic equilibrium after 10 ns of the simulation under the conditions employed. However, fluctuations of the RMSDs were still detectable even at around 30 ns of the simulations, suggesting that some regions of the outer domains continued to fluctuate.

To map the heavily fluctuating sites in the gp120 outer domain, we calculated the RMSF of the main chains of individual amino acids during the MD simulations. The RMSFs, which provide information about the atomic fluctuations during MD simulations [34], were found to be much greater in the amino acids constituting loops than those of the structured regions, such as helixes and β-sheets (Figs. 1C and 1D). These results are consistent with the general observations of proteins in solution, and indicate that the loops of the gp120 outer domain intrinsically possess structural flexibility in water. Notably, the RMSFs in some loops were markedly different between the two V3 recombinant gp120s. For example, the RMSF in the β20–β21 loop was much greater in the $Gp120_{LAI\text{-}TH09V3}$ (Fig. 1C). Conversely, those in the D loop were greater in the $Gp120_{LAI\text{-}NH1V3}$.

HIV-1 gp120 V3 loop often has a motif for the N-linked glycosylation that is usually preferentially conserved in R5 viruses (Fig. 1A). To address potential impacts of the glycan on the MD simulations, we performed MD simulation in the presence of a high mannose oligosaccharide in the V3 loop. We observed any significant differences in the structure and dynamics of gp120 outer domain in the presence or absence of the glycan (data not shown). This is reasonable because the glycosylation site is exposed toward an opposite direction from the gp120 core (Fig. 1D).

To clarify structural differences between the $Gp120_{LAI\text{-}NH1V3}$ and $Gp120_{LAI\text{-}TH09V3}$, we constructed their averaged structures using the 40,000 snapshots obtained from 10–30 ns of MD simulations using ptraj module in Amber 9. Superposition of the averaged structures showed that the relative configuration of the V3 loops and β20–β21 was markedly different between the two outer domains: the V3 tip protruded a greater distance from the β20-β21 loop in the $Gp120_{LAI\text{-}TH09V3}$ than in the $Gp120_{LAI\text{-}NH1V3}$ (Fig. 2A). The superposed structures also revealed differences in a region around the CD4 binding site (Fig. 2A, right panel with enlarged CD4 binding site). The relative configuration of the CD4 binding loop to the exit loop is critical for the gp120 binding to the CD4, a primary infection receptor of HIV-1 [17]. Therefore, we analyzed the distance between the CD4 binding and exit loops by measuring the distance ($D_{115-221}$) between the Cα of Gly115 and the Cα of Gly221 as an indicator (Fig. 2B). As expected from the fluctuations of the CD4 binding loop, the $D_{115-221}$ fluctuated during the MD simulations (Fig. 2C). However, the $D_{115-221}$ was significantly smaller in the $Gp120_{LAI\text{-}TH09V3}$ than in the $Gp120_{LAI\text{-}NH1V3}$ (Fig. 2D; $p<0.001$, Student's *t*-test): the $D_{115-221}$ ranged from 4–15 Å with an average of ~8 Å for the $Gp120_{LAI\text{-}TH09V3}$ and from 7–17 Å with an average of ~10 Å for the $Gp120_{LAI\text{-}NH1V3}$. These data suggest that the CD4 binding loop tended to be positioned more closely to the exit loop and thus tended to be sterically less exposed in the $Gp120_{LAI\text{-}TH09V3}$ than the $Gp120_{LAI\text{-}NH1V3}$.

Neutralization study

The above structural data raised the possibility that the reduction in the V3 net charge might reduce HIV-1 neutralization sensitivity by the anti-CD4 binding site antibodies. To address this possibility, we performed a neutralization assay using the two isogenic HIV-1 recombinant viruses, $HIV\text{-}1_{LAI\text{-}NH1V3}$ and $HIV\text{-}1_{LAI\text{-}TH09V3}$ [35], which carry the $Gp120_{LAI\text{-}NH1V3}$ and $Gp120_{LAI\text{-}TH09V3}$, respectively. These viruses were pre-incubated with various human MAbs against the CD4 binding site, and the reductions in viral infectious titers were measured using a HeLa-cell-based single-round viral infectivity assay system [36].

Table 1 summarizes the results of the neutralization assay. As expected, the two viruses exhibited markedly distinct neutralization sensitivities to the three human MAbs against the CD4 binding site. $HIV\text{-}1_{LAI\text{-}NH1V3}$ was consistently neutralized with all three MAbs against the CD4 binding site (49G2, 42F6, and 0.5δ), with ND_{50} values ranging between 0.224 and 0.934 μg/ml. In marked contrast, $HIV\text{-}1_{LAI\text{-}TH09V3}$ was highly resistant to neutralization by these MAbs, and 10 μg/ml of antibodies failed to block the viral infections. The two viruses were equally resistant to an anti-Gp120 antibody (4C11) that recognizes the Gp120 structure after CD4 binding. The result indicates that the CD4-induced gp120 epitope of the 4C11 are not preserved in the V3 recombinant viruses used in the present study. Conversely, they were equally sensitive to another ant-Gp120 antibody (4301 [37]) whose epitope is located outside of the CD4 binding site. A human MAb 8D11 used as a negative control had no effect on the viral infectivity in this assay.

Diversity study

Host immunity is a driving force behind the antigenic diversity of envelope proteins of the primate lentiviruses that establish persistent infection in hosts [23,38,39,40,41]. The above and

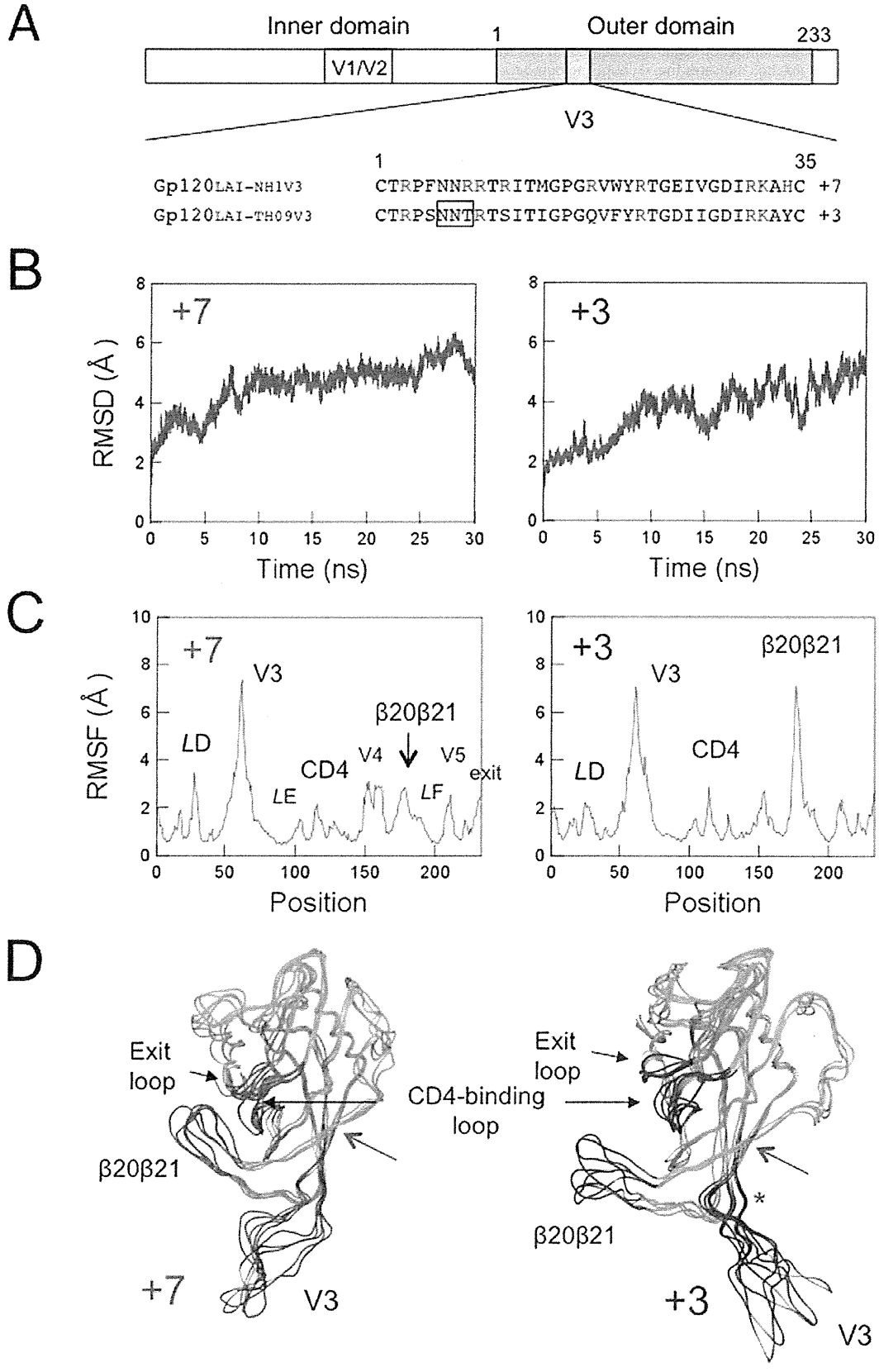
A
Inner domain
1
Outer domain
233
V1/V2
V3
1
35
Gp120LAI-NH1V3 CTRPFNNRRTRITMGPGRVWYRTGEIVGDIRKAHC +7
Gp120LAI-TH09V3 CTRPSNNTRTSITIGPGQVFYRTGDIIGDIRKAYC +3
B
+7
+3
RMSD (Å)
Time (ns)
C
+7
+3
RMSF (Å)
V3
β20β21
LD
CD4
V4
V5
exit
LE
LF
Position
D
Exit loop
CD4-binding loop
β20β21
+7
+3
V3

Figure 1. MD simulation of the identical gp120 outer domain carrying a V3 loop with net charge of +7 or +3. (A) Schematic representation of the gp120 open reading frame along with the amino acid sequences. The net charge indicates the number of positively charged amino acids (R, K, and H) minus the number of negatively charged amino acids (D and E) in the V3 loop. A light blue box indicates the outer domain used for the MD simulations. A pink box indicates the V3 loop. The numbers indicate amino acid positions at the outer domain (amino acids 1 to 233 in Figure 1A correspond to amino acids 256 to 489 in the gp120 of HIV-1_{LAI}) or the V3 loop. An open black box in the V3 loop sequence indicates a potential site for the N-linked glycosylation. (B–D) Left panels: $Gp120_{LAI\text{-}NH1V3}$; Right panels: $Gp120_{LAI\text{-}TH09V3}$. +7 and +3 indicate the net charges of V3 loops of the recombinant proteins. (B) Time course of RMSD during MD simulations. The RMSD values indicate the structural fluctuations of the outer domain in aqueous solution. The numbers in the horizontal axes indicate the time of MD simulation. (C) Distribution of RMSF in the gp120 outer domain. The RMSF values indicate the atomic fluctuations of the main chains of individual amino acids during 10–30 ns of MD simulations. The numbers in the horizontal axes indicate amino acid positions at the outer domain. (D) Superimposition of Gp120 models at 10, 15, 20, 25, and 30 ns of MD simulation. A green asterisk indicates approximate position of a potential N-glycosylation site at the V3 stem. A green arrow indicates the site of the disulfide bond at the V3 base.
doi:10.1371/journal.pone.0037530.g001

previous [12,13,14,15,16] neutralization studies raised the possibility that the gp120 surface might be less heterogeneous in gp120 subpopulations that have a less positively charged V3 loop, due to greater magnitudes of resistance to the antibody neutralization. To address this possibility, we performed an information entropy study using sequences in the public database. We extracted full-length gp120 amino acid sequences of HIV-1 subtype CRF01_AE that has the same evolutionary origin and is spread throughout southeast Asia [42]), and divided them into subgroups on the basis of the net charge of V3 loop (+2, +3, +4, +5, +6, +7, and +8). The sequences were used to calculate the Shannon entropy scores, *H(i)* [1], to denote the diversity of individual amino acids within each subpopulation.

Figure 3 shows the 3-D distribution of the *H(i)* scores of individual amino acids plotted on the HIV-1 gp120 crystal structure (PDB code: 2B4C [1]), where the green to orange regions were suggested to have more variable amino acids than the blue ones. In the gp120 subpopulation that has +7 V3 loop, the *H(i)* scores often exceeded 2.0 bits at many residues, reaching close to the maximum value of 4.4, i.e., the diversity was maximal, at the V5 region (Fig. 3A, left panel). Regions with high *H(i)* scores included the functional sites, such as the V3 loop and the regions around the CD4 binding site. In marked contrast, in the gp120 subpopulation carrying the +3 V3 loop, the *H(i)* scores were almost zero, i.e., the diversity was minimal, at many amino acids, but not at those in the V4, V5, and *L*E regions (Fig. 3A, right panel). Importantly, relatively high levels of conservation were also detected with amino acids in the otherwise highly variable V3 loop. Moreover, a region adjacent to the CD4 binding loop was also less heterogeneous compared with those of the gp120 subpopulation carrying +7 V3 loop (Figs. 3B). In the gp120 subpopulations carrying the +2, +3, 4, and +5 V3 loops, the *H(i)* scores were indistinguishable from each other: they were less heterogeneous than the subpopulations carrying the +6, +7, and +8 V3 loops. Similar results were obtained with HIV-1 subtype C that represents the most predominated HIV-1 in the world (data not shown).

Discussion

The ability of HIV-1 to rapidly change its phenotype greatly complicates our efforts to eradicate this virus. Elucidation of structural principles for the phenotypic change may provide a clue to control HIV-1. In this study, by combining MD simulations with antibody neutralization experiments and diversity analysis of the viral protein sequences, we studied a structural basis for the phenotypic change of HIV-1 by V3 mutations. To address this issue, we used a V3 recombinant system; we performed a computer-assisted structural study and an infection-based neutralization assay using gp120 proteins whose amino acid sequences are identical except for V3 loop. In combination with an informatics study, we obtained evidence that the HIV-1 V3 loop acts as an electrostatic modulator that influences the global structure and diversity of the interaction surface of the gp120 outer domain.

Using MD simulation, we first examined whether the V3 net charge could affect the structural dynamics of the HIV-1 gp120 outer domain surface. Initial structures of the outer domain of the two gp120s, $Gp120_{LAI\text{-}NH1V3}$ and $Gp120_{LAI\text{-}TH09V3}$, were identical before MD simulations, because the domains were both derived from HIV-1_{LAI} strain. Remarkably, however, the two molecules with distinct V3 loop exhibited markedly distinct structural dynamics following MD simulations (Figs. 1 and 2). These data strongly suggest that the V3 net charge can act as an intrinsic modulator that influences the structural dynamics of the interaction surface of the gp120 outer domain. Such a global effect on structure by a local electrostatic change has been reported with bacteriorhodopsin [43]. In general, the long-range effects of non-electrostatic contributions are negligible, whereas those of the electrostatic contributions are not [34]. Therefore, it is reasonable that the changes in overall charge of the V3 loop element caused the global effects on the gp120 structure via alteration of the electrostatic potentials of the gp120 surface.

We next studied biological impact of the structural changes predicted by MD simulations. The MD simulations suggested that the CD4 binding loop was less exposed in the $Gp120_{LAI\text{-}NH1V3}$ than the $Gp120_{LAI\text{-}NH1V3}$ (Fig. 2). The finding predicted that reduction in V3 net charge could cause reduction in neutralization sensitivity to the anti-CD4 binding site antibodies. This possibility was assessed by neutralization assay. We used infectious HIV-1_{LAI} clones having the $Gp120_{LAI\text{-}NH1V3}$ or the $Gp120_{LAI\text{-}TH09V3}$ to assess their neutralization sensitivities to the anti-CD4 binding site MAbs. Notably, we indeed observed marked reduction in the neutralization sensitivity in HIV-1_{LAI} having $Gp120_{LAI\text{-}TH09V3}$ (Table 1). The results are consistent with the structural changes predicted by MD simulations, as well as previous findings on neutralization sensitivity of HIV-1s to soluble CD4 [14,15,16].

We further studied evolutionary impact predicted by MD simulations and the neutralization studies. These studies predicted that reduction in V3 net charge could cause reduction in sequence diversity around the CD4 binding site due to reduced sensitivity to positive selection pressures of antibodies. Notably, we indeed observed marked reduction in the gp120 diversity: our Shannon entropy data show that otherwise variable surfaces of gp120, such as V3 and a region around the CD4 binding loop, are less heterogeneous in the gp120 subgroups carrying a V3 loop with a +3 charge (Fig. 3).

Previous cryo-electron microscopy studies have indicated that gp120 forms a trimer on an HIV-1 virion, where the CD4 binding sites are exposed on the outside surface in the solution [44,45,46]. Therefore, it is reasonable that gp120 with +3 V3 with less exposed CD4 binding loop is less sensitive to neutralization by anti-CD4 binding site antibodies (Table 1) and less heterogeneous around the CD4 binding site (Fig. 3). Collectively, our results

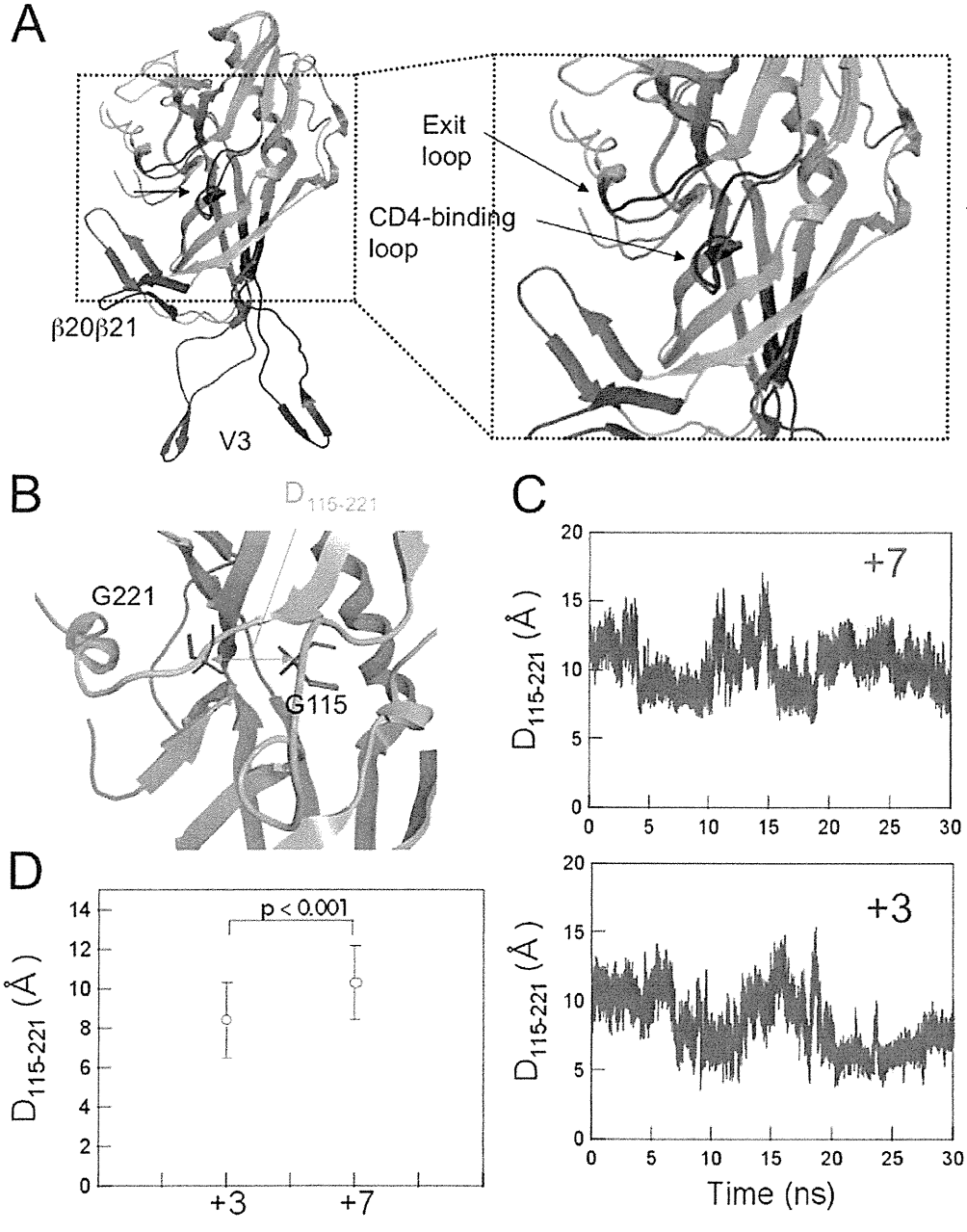

Figure 2. Comparison of the averaged 3-D models during MD simulation. (A) Superposition of the averaged structures obtained with the 40,000 snapshots obtained from 10–30 ns of MD simulations using ptraj module in Amber 9. Red and Blue ribbons: loops of $Gp120_{LAI\text{-}NH1V3}$ and $Gp120_{LAI\text{-}TH09V3}$ with V3 net charges of +7 and +3, respectively. (B–D) Configuration and structural dynamics of the CD4 binding loop. The distance between the Cα of Gly115 and the Cα of Gly221 in the CD4 binding loop was calculated to monitor configurational changes (B). The distance was monitored during the 10–30 ns of MD simulation (C) and the average distance with variance was plotted (D). +7: $Gp120_{LAI\text{-}NH1V3}$; +3: $Gp120_{LAI\text{-}TH09V3}$.
doi:10.1371/journal.pone.0037530.g002

obtained with all three approaches agree with each other and suggest that V3 net charge is an intrinsic factor that influences structural property, antibody sensitivity, and sequence diversity of CD4 binding site.

The HIV-1 gp120 outer domain has several functional or immunogenic loops involved in binding to CD4, coreceptor and antibodies. Our MD simulations predicted that V3 net charge influences fluctuation and conformation of these loops (Figs. 1 and 2). The V3-based structural modulation of the gp120 surface loops may be an effective mechanism to alter effectively the phenotype and relative fitness of HIV-1. For example, a change in the V3 net charge by mutations may induce changes in V3 conformation (Figs. 1D and 2A) [13], which in turn may influence intra- or inter-molecular interactions among gp120 monomers and thus global structure of gp120 trimer on a virion. Generation of a swarm of structural variants by V3 mutations could help generating the best-

Table 1. Neutralization sensitivity of the isogenic V3 recombinant HIV-1 to anti-gp120 monoclonal antibodies.

Antibody ID	Ig subtype	Epitopes on Gp120	ND_{50} (μg/ml)[@]	
			$HIV\text{-}1_{LAI\text{-}NH1V3}$	$HIV\text{-}1_{LAI\text{-}TH09V3}$
49G2	human IgG1	CD4 binding site[#]	0.224	>10
42F9	human IgG1	CD4 binding site[#]	0.934	>10
0.5δ [59]	human IgG1	CD4 binding site[#]	0.444	>10
4C11 [59]	human IgG2	CD4 induced structure[$]	>20	>10
4301	mouse IgG	broadly reactive*	0.59	0.57
8D11	human IgG1	none	>20	>10

[#]Neutralization epitope in the Gp120 outer domain before CD4 binding.
[$]Neutralization epitope induced in Gp120 after CD4 binding.
*Epitopes outside of the CD4 binding site [37].
[@]The effect of each antibody on viral infectivity was tested in duplicate.
doi:10.1371/journal.pone.0037530.t001

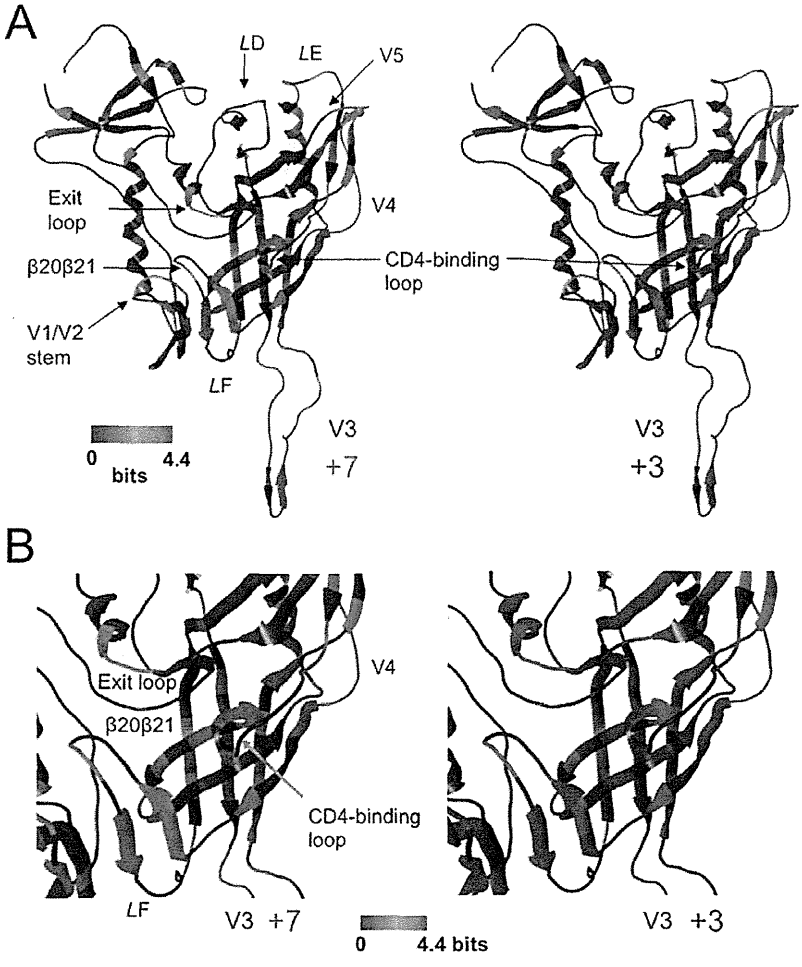

Figure 3. Diversity of the gp120 subpopulations carrying a V3 loop with net charge of +7 or +3. Full-length gp120 sequences of the HIV-1 CRF01_AE [42] were extracted from a public database, and divided into subgroups on the basis of the net charge of the V3 loop (+2~+8). The divided sequences were used to calculate the Shannon entropy, *H(i)* [63], within each subpopulation, and the *H(i)* values were plotted on the 3-D structure of gp120 (PDB code: 2B4C [1]). The results for the gp120 subgroups that have V3 loops with +7 (left panel) and +3 (right panel) charges are shown as representative. The numbers of sequences used to calculate the *H(i)* were 9 and 81 for +7 and +3, respectively. (A) Distribution of *H(i)* in the gp120 monomer. (B) Distribution of *H(i)* around the CD4 binding site.
doi:10.1371/journal.pone.0037530.g003

fit variants under changing environments during persistent infection of HIV-1 *in vivo*. Further study is necessary to address above issue.

Thus far fine structures of neither the intact gp120 monomer nor trimer are available. However, recent crystal structure study disclosed a structure of V1/V2 domain [47], which had been the major gp120 region lacking structural information. The V1/V2 domain is located on the outer surface of gp120, as is V3, and can participate in phenotypic changes of HIV-1 [48,49]. In this regard, Kwon et al [50] have found an intriguing role of gp120 variable loops; gp120 core has an intrinsic preference to form the CD4-bound conformation, whereas the variable loops, such as V1/V2 and V3 loops, play key roles in preventing conformational transitions into the CD4-bound state that is sensitive to neutralization. Thus it is conceivable that configurational changes of V3 loop by V3 mutations play roles in modulating structural dynamics of the unliganded gp120 core and neutralization sensitivity of HIV-1. Availability of the V1/V2 loop structure will promote structural study of the whole gp120 monomer containing V3 loop, V1/V2 domain, and glycans. Our findings will provide a structural basis to elucidate intra-molecular interactions of these elements, which in turn will allow the study of structure, function, and evolution of gp120 trimer. Incorporation of MD simulation into these studies will help understanding structural dynamics with which HIV-1 adjusts its relative replication fitness in nature.

Materials and Methods

Characteristics of the gp120 proteins and HIV-1s used

We used two isogenic recombinant gp120 proteins, termed $Gp120_{LAI\text{-}NH1V3}$ and $Gp120_{LAI\text{-}TH09V3}$ [35], for the present structural and neutralization studies. They differ only in their V3 loops. The $Gp120_{LAI\text{-}NH1V3}$ and $Gp120_{LAI\text{-}TH09V3}$ have the 35-amino-acid-length V3 loops from HIV-1-infected individuals in the gp120 backbone of the $HIV\text{-}1_{LAI}$ strain [35]. The net charges of the V3 loops are +7 and +3 for the $Gp120_{LAI\text{-}NH1V3}$ and $Gp120_{LAI\text{-}TH09V3}$, respectively (the V3 net charge represents the number of positively charged amino acids (R, K, and H) minus the number of negatively charged amino acids (D and E) in the V3 loop). The $HIV\text{-}1_{LAI}$ carrying the $Gp120_{LAI\text{-}NH1V3}$ ($HIV\text{-}1_{LAI\text{-}NH1V3}$) is the CXCR4 tropic virus, whereas that carrying the $Gp120_{LAI\text{-}TH09V3}$ ($HIV\text{-}1_{LAI\text{-}TH09V3}$) is the CCR5 monotropic virus [35]. The $HIV\text{-}1_{LAI\text{-}NH1V3}$ is sensitive to neutralization by antibodies with the ability to bind to the peptides containing the autologous V3 tip sequences, whereas $HIV\text{-}1_{LAI\text{-}TH09V3}$ is highly resistant to antibodies targeting the autologous V3 tip sequences [13].

MD simulation

As the initial structures for the MD simulation, we first constructed three-dimensional (3-D) models of the outer domains of the $Gp120_{LAI\text{-}NH1V3}$ and $Gp120_{LAI\text{-}TH09V3}$ by the comparative (homology) modeling method (reviewed in [33,51,52]), as described previously [13]. We used the crystal structure of HIV-1 gp120 containing an entire V3 region at a resolution of 3.30 Å (PDB code: 2B4C [1]) as the modeling template. The gp120 core is in complex with the CD4 receptor and the CD4 induced structure (CD4i) antibody X5 [1]: it represents the structure after the CD4 binding. We deleted the structures of the CD4 receptor and the X5 antibody from the 2B4C complex structure to construct the free gp120 outer domain models of $HIV\text{-}1_{LAI}$ V3 recombinant viruses by homology modeling. Then the models were subjected to the MD simulations to analyze structure and dynamics of the gp120 outer domain in the absence of the CD4 receptor and the X5 antibody interactions. The homology modeling was performed using tools available in the Molecular Operating Environment (MOE) program (MOE 2008.10; Chemical Computing Group Inc., Montreal, Quebec, Canada). The 186 amino-terminal and 27 carboxyl-terminal residues were deleted to construct the gp120 outer domain structure. We optimized the 3-D structure thermodynamically via energy minimization using an MOE and an AMBER99 force field [53]. We further refined the physically unacceptable local structure of the models based on a Ramachandran plot evaluation using MOE. MD simulations were performed as described previously [13] using the Sander module in the Amber 9 program package [54] and the AMBER99SB force field [55] with the TIP3P water model [56]. Bond lengths involving hydrogen were constrained with the SHAKE algorithm [57], and the time step for all MD simulations was set to 2 fs. A nonbonded cutoff of 12 Å was used. After heating calculations for 20 ps to 310 K using the NVT ensemble, the simulations were executed using the NPT ensemble at 1 atm at 310 K for 30 ns. Superimpositions of the $Gp120_{LAI\text{-}NH1V3}$ and $Gp120_{LAI\text{-}TH09V3}$ structures were done by coordinating atoms of amino acids along the β-sheet at the gp120 outer domain. We performed two independent MD simulations with distinct MD codes and obtained similar results. Therefore, we present here the data set from one of the MD simulations as a representation.

Calculation of the root mean square deviation (RMSD) and root mean square fluctuation (RMSF)

The RMSD values between the heavy atoms of the two superposed proteins were used to measure the overall structural differences between the two proteins [34]. We also calculated the RMSF to provide information about the atomic fluctuations during MD simulations [34]. In this study, we calculated the RMSF of the main chains of individual amino acids using the 40,000 snapshots obtained from MD simulations of 10–30 ns. The average structures during the last 20 ns of MD simulations were used as reference structures for the calculation of the RMSF. Both the RMSD and RMSF were calculated using the ptraj module in Amber 9 [34].

Monoclonal antibodies (MAbs)

The 49G2, 42F9, 0.5δ and 4C11 antibodies used for the neutralization assay were the human MAbs established from an HIV-1-infected patient with long-term non-progressive illness. Human blood samples were collected after signed informed consent in accordance with study protocol and informed consent reviewed and approved by Ethics committee for clinical research & advanced medical technology at the Faculty of Life Science Kumamoto University. B cells from the patient's peripheral blood mononuclear cells were transformed by EBV, followed by cloning as described previously [58]. The culture supernatant from an individual clone was screened for the reactivity to $gp120_{SF2}$ by an enzyme-linked immunosorbent assay (ELISA). The specificity of antibodies was determined by gp120 capture ELISA and FACS analysis as described previously [59]. Briefly, reactivity of the mAbs against monomeric gp120 of $HIV\text{-}1_{SF2}$ was measured with a gp120 capture assay in the absence or presence of soluble CD4 (0.5 μg/ml). Decrease in the binding activity was observed for the mAbs 0.5δ, 49G2, and 42F9 in the presence of soluble CD4, whereas enhancement in the reactivity was detected for the mAb 4C11. Reactivity of the mAbs against envelope protein on the cell surface was measured with a FACS analysis of PM1 cells chronically infected with JR-FL in the absence or presence of soluble CD4 (0.5 μg/ml). No significant difference was observed for the binding profiles of 0.5δ, 49G2, and 42F9 in the presence of